Food aeration: effect of the surface-active agent type on bubble deformation and break-up in a viscous Newtonian fluid: from single bubble to process-scale

B. Sanogo, K. Souidi, Alain Marcati, C. Vial

HIGHLIGHTS

- Food aeration at pilot scale was investigated using two technologies and three surfactants.
- Whey proteins (WPC) are a better foaming agent than sodium caseinate (SCN) and tween 20 (TW20).
- Experimental data were confronted to the visualization of single bubble break-up under shear flow.
- WPC and SCN promoted bubble break-up by *tip streaming*; TW20 only deformed bubbles.
- Single bubble break-up needs higher shear with WPC than SCN, but kinetic limitations appear with SCN during aeration.

Food aeration: effect of the surface-active agent type on bubble deformation and break-up in a viscous Newtonian fluid: from single bubble to process-scale

B. SANOGO[1*], K. SOUIDI[1,2], A. MARCATI[1], C. VIAL[1]

[1]Université Clermont Auvergne, CNRS, Clermont Auvergne INP, Institut Pascal, F-63000, Clermont-Ferrand, France

[2]Université La Réunion, CIRAD, Université Montpellier, Institut Agro Montpellier, IRD, Université Avignon, Qualisud, F-97490 Sainte Clotilde, France

*Corresponding author: boubakar.sanogo@uca.fr

Abstract

Two continuous whipping devices, a rotor-stator (RS) and a narrow angular gap unit (NAGU), were used to produce aerated food with a 25% (v/v) gas fraction target. The liquid phase was a Newtonian model-solution containing 2% (w/w) of either whey proteins (WPC), sodium caseinate (SCN), or tween 20 (TW20). Strong differences emerged regarding gas incorporation and bubble size as a function of process parameters: namely, rotation speed and residence time. To improve understanding of the results obtained at pilot-scale, a second investigation consisting in the observation of the deformation and break-up of single gas bubbles has been undertaken using successively a Couette device and an impeller close to NAGU. For proteins, the observation of single bubble deformation and break-up showed that bubble break-up occurred by *tip-streaming* above a well-defined critical Capillary number Ca_c of 0.27 and 0.5 for SCN and WPC, respectively, whereas no break-up was observed with TW20 even though Ca reached 10. The poor foaming ability obtained with TW20 could be explained by a poor break-up mechanism, promoting coalescence and gas plugs at high shear instead of gas incorporation. Conversely, protein promote tip-streaming as the major break-up mechanism at low shear rate, explaining why rotation speed is not a key process parameter. Differences observed between SCN and WPC can be attributed to diffusion limitation for SCN when a much larger surface area is generated during aeration.

Keywords: continuous aeration process, bubble break-up, tip-streaming, simple shear flow, protein, surfactant

Nomenclature

Dimensionless numbers

Ca: Capillary number
Ca_c: critical Capillary number
Re: Reynolds number

Abbreviations

BSA: bovine serum albumin
BSD: bubble size distribution
HMW: high molecular weight
LMW: low molecular weight
NAGU: narrow angular gap unit device
RS: rotor-stator device
SAA: surface-active agent
SCN: sodium caseinate
TW20: tween 20
WPC: whey protein concentrate

Greek symbols

$\dot{\gamma}$: shear rate (s^{-1})
ε: experimental gas volume fraction (%)
ε_{max}: theoretical gas volume fraction (%)
η_c: viscosity of the continuous phase (Pa.s)
λ: viscosity ratio (-)
ρ_i: liquid density ($kg.m^{-3}$)
ρ_f: foam density ($kg.m^{-3}$)
σ: equilibrium surface tension ($N.m^{-1}$)
τ: shear stress (Pa)

Latin characters

a: radius of the initial bubble (m)
B: half-length of the minor axis (m)
D: deformation parameter (-)
D_{in}: initial bubble diameter (m)
D_{mean}: average bubble diameter (m)
$e_{Couette}$: gap between cylinders (m)
G_i: gas flow rate ($m^3.s^{-1}$)
L: half-length of the major axis (m)
L_i: liquid flow rate ($m^3.s^{-1}$)
N: rotor speed (s^{-1})
R_i: radius of inner cylinder (m)
$\bar{t}$: residence time (s)

1. INTRODUCTION

Foam-based products are found and very common in the food industry with products such as cake batter, ice-cream, whipped cream, etc. Foams are a dispersion of gas bubbles in a liquid or solid matrix [Stevenson, 2012; Cantat et al., 2013]. During the foaming process, mechanical shearing forces are typically employed to break the dispersed gas phase into small bubbles, leading to a substantial increase in surface area. Adding surface-active agents (SAA) is an effective approach to reduce surface tension [Ho et al., 2021] by decreasing the work required to generate foams. There has been a huge number of published papers on food aeration, focused on the properties of SAA [Bezelgues et al.,2008; Zhang et al., 2013], the rheology of the fluid phases as well as surface tension [Séguineau de Préval et al., 2014; Mezdour et al., 2017], the geometry of the processing apparatus [Müller-Fischer and Windhab, 2005; Narchi et al., 2011], and the specific processing parameters [Jabarkhyl et al., 2020; Badve, 2021]. Most of these studies investigated food aeration with a "black-box" approach at pilot-scale, i.e., analyzing the effect of process parameters on the overrun and stability of the foams produced without focusing on how the gas phase is dispersed inside the foaming device. There is still, however, much to understand regarding the primary break-up of bubbles during aeration. Understanding this primary break-up process could play a significant role in improving foam formation. A common starting point is the break-up of a single bubble.

The break-up of a single bubble or droplet has been a topic of long-term interest due to the common appearance of this phenomenon in various fields of engineering (food processing, emulsion formation, aerosols, etc.). A pioneering investigation of steady simple shear flows was performed by Taylor [1932; 1934]. It was found that when inertia is negligible, i.e., very low Reynolds number (*Re*), the deformation of the drop prior to its break-up is mainly governed by the viscosity ratio (λ) of the phases and the Capillary number (*Ca*). *Ca* is the ratio between the viscous stress which acts to deform the bubble and the stabilizing Laplace pressure. *Ca* is defined by Eq. (1) where η_c is the liquid viscosity, $\dot{\gamma}$ the shear rate, d_i the bubble initial diameter, and σ the equilibrium surface tension.

$$Ca = \frac{\eta_c \, \dot{\gamma} \, d_i}{2\sigma} \tag{1}$$

Taylor [1934] also introduced the deformation parameter *D* Eq. (2) frequently used for small deformations (*Ca* << 1) where *L* is the half-length of the major axis and *B* the half-length of the minor axis of the deformed (ellipsoidal) bubble.

$$D = \frac{L - B}{L + B} \tag{2}$$

For *Ca* << 1 and λ << 1, the bubble is nearly spherical with $D \approx Ca$. This theory has been fully validated by experiments [Torza et al., 1971] and numerical simulations [Rallison, 1981].
At large deformation (*Ca* >> 1), *D* tends to a limiting value of 1 and becomes useless. Beyond, the parameter *L/a* must be used to measure the deformation (*a* is the initial nondeformed bubble radius). A power law was often proposed to correlate the *L/a* parameter to *Ca*:

$$\frac{L}{a} = \alpha \, Ca^{\beta} \tag{3}$$

where α and β are constants. Using the slender body theory and assuming that bubbles are circular in cross section, Hinch and Acrivos [1980] predicted for *Ca* >> 1, λ << 1, and *Re* << 1 that:

$$\frac{L}{a} = 3.45\, Ca^{0.5} \quad (4)$$

Canedo et al. [1993] studied experimentally the deformation of air bubbles suspended in polybutene in a Couette device and found that bubble cross-sections were elliptical and suggested a slightly different law of deformations versus *Ca* (range 3 to 50):

$$\frac{L}{a} = 3.1\, Ca^{0.43} \quad (5)$$

Rust and Manga [2002] and Müller-Fischer et al. [2008] performed the most recent studies on bubble behavior under stress. Rust and Manga [2002] were interested in the measurements of the shape and orientation of air bubbles in a viscous Newtonian fluid deformed by simple shear. Their data indicated that for extremely small *Re* and λ, the deformation parameter *D* was a good approximation for $Ca < 0.5$. Müller-Fischer et al. [2008] used two different visualization devices to monitor bubble behavior in simple shear until break-up occurs.

A bubble in a steady flow deforms until the interfacial stress which holds it together can no longer counterbalance the viscous stresses. *Ca* value at which the deformation becomes unsteady, leading to the break-up of the bubble, is called the critical Capillary number (Ca_c). Grace [1982] conducted a thorough experimental investigation on the deformation and the break-up of droplets accounting for a wide range of viscosity ratios ($10^{-6} < \lambda < 10^{3}$) and found that Ca_c strongly depends on λ. Regarding these phenomena, Rumscheidt and Mason [1961] distinguished the different deformation and break-up mechanisms of droplets in shear flows, presenting three break-up modes. The first is a droplet-breaking mode by the tips called *tip-streaming*. In the second case, the drop breaks by the *binary break-up* mode, splitting into two daughter drops. In the third case, the drop extends to a long thread that breaks after a long time. Rumscheidt and Mason [1961] concluded that λ is the most important parameter determining the break-up type. De Bruijn [1993] analyzed the cause of *tip-streaming*: interfacial tension gradients developed on the drops, resulting in a low interfacial tension at the tips and a higher tension elsewhere. According to the author, this phenomenon occurs when there is a moderate level of the SAA. Most of the results regarding break-up phenomena cited above are related to drops and not bubbles; in this case λ is far smaller due to the low gas density. Furthermore, the role of SAA such as proteins on single bubbles deformation and break-up has been poorly investigated.

It is commonly admitted for dry foams that their stability is strongly linked to the interfacial properties of the adsorbed layers, in particular to their rheological properties, such as the surface viscoelasticity of protein films on the one hand, or the Gibbs-Marangoni mechanism for low-molecular-weight surfactants on the other hand. Their role on single bubbles deformation and break-up in a liquid phase has, however, been poorly studied in comparison to single drops. Even though these properties play obviously a key role in foaming properties from the laboratory scale to the industrial scale, no quantitative approach has been able to link foaming efficiency and interfacial properties up to now. From qualitative analysis, it is clear that if an enhanced interfacial rigidity may be necessary to improve long-term foam stability, this should not prevent bubbles break-up during foam formation. This means that the control of the respective dynamics of shear-induced bubble break-up and interfacial mechanisms able to increase interface rigidity and stability is pivotal for to a successful aeration process. While recent advances in interfacial rheological properties in the nonlinear domain could help reach a better understanding [Bykov et al., 2015], experimental

techniques remain, however, limited to a too low-frequency domain in comparison to industrial conditions.

Extensive literature can be found regarding protein-stabilized gas-liquid interfaces in foams [Zhan et al., 2022] but it is also important to investigate the origins of the foamability of protein solutions. Souidi et al. [2012] investigated the mechanisms of bubble break-up with food model solutions containing whey proteins. *Tip-streaming* was identified as the main bubble break-up mode, and this was associated with a narrow bubble size distribution in the foams obtained with this protein solution in the range between 25 and 50% (v/v) gas fraction. These conclusions raised an important question: is this break-up mode related to the specific operating conditions (i.e., shear flow in laminar conditions at a low viscosity ratio) whatever the SAA, or is this break-up mode depends on the nature of the SAA (i.e., whey proteins) used?

In order to answer these questions, this paper aims to study the deformation and break-up mechanisms under shear flow of bubbles stabilized by three different SAA. Whey protein concentrate (WPC), sodium caseinate (SCN), and tween 20 (TW20) were used in Newtonian model-solutions with controlled bulk viscosity and at the same weight percentage. WPC and SCN have nearly the same average molecular weight (14-25 kDa) but not the same structure: whey proteins are globular proteins, whereas caseins have a flexible structure [Fox et al., 2017]. TW20 was selected as a low-molecular-weight (LMW) surfactant to extend the range of SAA's type and molecular weight. The three model-solutions were also used to carry out aeration with two different pilot-scale apparatus. The objective was to investigate how the SAA affects single bubble break-up mode and to establish a relationship between aeration and single bubble break-up data.

2. MATERIAL AND METHODS

2.1. Raw materials

In this study, model-fluids consisting of dehydrated glucose syrup and SAA were used to tailor physicochemical properties (viscosity, surface properties) close to food media. The glucose-dried powder (Glucidex IT21) used was obtained from *Roquette Frères* (France). Three different SAA were used:

- Whey protein concentrate (WPC, Protarmor 80) was obtained from *Armor Proteins* (France). This concentrate with a high nutritional value is assumed free of lactose and fat. WPC contains 85% (w/w) protein material consisting of 75% β-lactoglobulin, 6% α-lactalbumin, and the rest as BSA and immunoglobulins. It is used as a foaming agent in the production of abundant and stable foams.
- Sodium caseinate (SCN) was also provided by *Armor Proteins* (France). SCN is a highly purified caseinate protein (91% w/w) used in the food industry as an emulsifier and/or a stabilizer [Einhorn-Stoll et al., 2002].
- Tween 20 (*Sigma-Aldrich Co.,* Germany) is a non-ionic surfactant based on aliphatic fatty acid esters having a hydrophilic-lipophilic balance (HLB) of 16.7. In the food industry, Tween 20 (TW20) is mainly used in frozen cream. It is known to form dry foams and enhance the stabilization of interfaces by steric forces [Samanta and Ghosh, 2011].

The model-fluids were prepared by dispersing 2% (w/w) SAA (WPC or SCN or TW20) in tap water (34 to 38% w/w) using an electric mixer (2.5 L Stephan UMC 5, Germany) at 300 rpm and room

temperature. Then, glucose syrup powder (60 to 64% w/w) was added to the SAA solutions, the mixture was homogenized at 1000 rpm for 30 minutes. Sodium azide NaN_3 (0.02% w/w) was finally added to the solutions to prevent microbial activities. Once prepared, the solutions were stored at 4°C for 48 hrs. for degassing and ensuring full hydration. After aging, they were characterized in terms of density (ρ_i), rheological properties (η) and equilibrium surface tension (σ).

2.2. Characterization of the model-fluids

The density of the model-fluids was measured by filling a crystallizer (*Duran*) of known volume; the whole was then weighed with a balance *(New Classic ML*, Mettler Toledo, Switzerland). The same procedure was followed for foams density measurements.

Rheological measurements were performed using a stress-controlled rheometer (AR G2*, TA instrument*, USA) equipped with a Peltier circulator for temperature control. Flow curves were obtained by monitoring shear stress (τ) as a response from 0.1 to 1000 s^{-1} shear rate ($\dot{\gamma}$) ramp. All tests were performed using a parallel-plate geometry (40 mm diameter; 1000 µm gap). The temperature was maintained at 20°C during measurements. Newtonian model was applied.

The equilibrium surface tension of the prepared solutions was measured using a tensiometer (K12, *Krüss GmbH*, Germany) equipped with a Wilhelmy platinum plate. The measurements were performed at a constant temperature (20°C) without sample dilution. The measurements were adapted to the SAA: 1 min for TW20 solution and at least 1 hr. for protein solutions.

All these measurements were done in triplicate and the average values are reported in Table 1.

Table 1: Physicochemical properties of the model-fluids.

SAA	Viscosity (Pa.s)	Surface tension (mN/m)	Density (kg/m^3)
WPC	1.1 ± 0.1	50.4 ± 0.3	1280 ± 10
SCN	0.92 ± 0.03	55.4 ± 0.3	1360 ± 10
TW20	0.84 ± 0.06	35.2 ± 0.2	1350 ± 30

2.3. Continuous foaming apparatus and conditions

Two types of continuous aeration devices were used to produce foams:

- a Narrow Angular Gap Unit (NAGU) consisting of a 3 stage-jacketed cylindrical stainless-steel column of 35 mm diameter (Fig. 1a). Each stage is mechanically stirred using seven right-angle mixing elements of 33 mm diameter. The compact and shifted configuration of the impellers was used to achieve efficient gas incorporation [Souidi et al., 2012].
- a Rotor-Stator (RS) consisting of a 35 mm diameter stator and a 15 mm diameter rotor, both fitted with seven rows of squared pins of 7.5 mm length resulting in a pin-to-wall gap of 2.5 mm (Fig. 1b). This geometry corresponds to the scale-down of typical aeration equipment of the food industry.

More details can be found in Narchi et al. [2011].

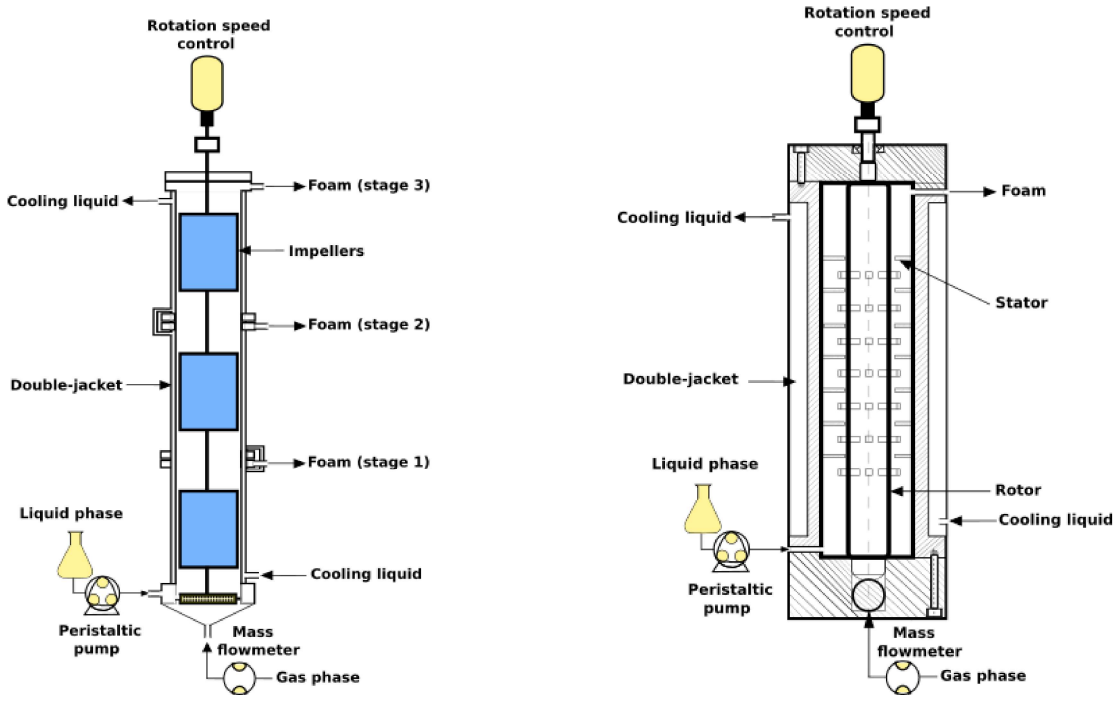

Figure 1: Schematic description of the experimental setups. (a) Narrow angular gap unit (NAGU) (b) Rotor-Stator (RS).

The liquid phase was supplied using a peristaltic pump (Masterflex L/S, *Cole-Parmer Instr. Co.*, USA) and the gas phase was supplied by a mass flow controller (*Emerson Brooks Inst.*, USA) in standard temperature and pressure (STP) conditions. Liquid was introduced by a side inlet in both devices, while gas was introduced through a sinter plate in NAGU and laterally in RS without sinter due to the configuration of the device. The impeller rotation speed (N) could vary from 10 to 1200 rpm using a speed-controlled motor (Janke Kunkel RE 16, *Ika-Werke GmbH,* Germany). Experiments were carried out at atmospheric pressure and the temperature was maintained at 20 °C. Steady-state conditions were achieved when the foam density value remained constant for three successive measurements.

In both devices, the reference gas (G_i) and liquid (L_i) volumetric flow rates were set at 10 mL/min and 30 mL/min respectively. The maximum theoretical gas fraction ε_{max} is 25% (v/v) (Eq. 6), which had been shown to be an adequate gas fraction for optimal gas dispersion [Narchi et al., 2011].

$$\varepsilon_{max} = \frac{G_i}{G_i + L_i} \tag{6}$$

Foaming efficiency is then calculated by dividing the actual gas fraction to its maximum value:

$$Foaming\ efficiency = \frac{\varepsilon}{\varepsilon_{max}} \tag{7}$$

Foam gas volume fraction (ε) was calculated using the density of the model-fluid and foam (ρ_i and ρ_f):

$$\varepsilon = \frac{\rho_i - \rho_f}{\rho_i} \quad (8)$$

Online image analysis consisting of a CCD camera coupled to a microscope (Axiovert-25, *Carl Zeiss Jena GmbH*, Germany) was used to measure bubble size distribution. Images were processed by free software *ImageJ* to determine bubble size. At least 500 bubbles were analyzed to avoid statistical bias and average bubble size was expressed considering the average diameter (D_{mean}) (Eq. 9) with n the number of bubbles and D_i the individual bubble diameter:

$$D_{mean} = \frac{\sum_{i=1}^{n} D_i}{n} \quad (9)$$

The effect of residence time inside the foaming devices was also assessed. For NAGU, it was possible by taking samples at the end of each stage. Concerning RS, volumetric flow rate conditions were reduced to G_i = 3.3 and L_i = 10 mL/min to increase residence time by a factor 3. Table 2 summarizes the process parameters related to flow conditions and rotation speed in both devices.

Table 2: Main characteristics of the two foaming devices.

Parameters	**NAGU**	**RS**
Maximum shear rate $\dot{\gamma}_{max}$ (s^{-1}) at 1200 rpm*	2200	880
Volume mean shear rate $\dot{\gamma}_{mean}$ (s^{-1}) at 1200 rpm**	386	364
Residence time $(\bar{t})$ (s) - 1 stage; G_i/L_i = 10/30***	188	270
Residence time $(\bar{t})$ (s) - 3 stages; G_i/L_i = 10/30	564	-
Residence time $(\bar{t})$ (s) - 1 stage; G_i/L_i = 3.3/10	-	812

**Maximum shear rate is calculated with the Couette approximation*
***Volume mean shear rate is calculated with the Metzner and Otto approximation*
**** Residence time considered as the reference*

2.4. Single-bubble visualization

The visualization system (Fig. 2) is a transparent Couette device developed by Souidi et al. [2012]. It consists of 35 mm diameter cylinder as a stator and an inner cylinder of 31 mm diameter (as a rotor). The model-solutions were filled in the remaining 2 mm gap ($e_{Couette}$) between the two cylinders, then gas bubbles were inserted from a syringe (*Hamilton Company*, USA) connected to a 180 mm (internal diameter) capillary tube (*Postnova Analytics GmbH*, Germany). The gas volumetric flow rate was controlled by a syringe pump (*KD scientific*, USA). A squared shape transparent box filled with the model-solution was added to prevent optical distortion. The entire device was illuminated by a continuous light source of 15 W (SBACK II, *TPL Vision*, France) to provide good recording conditions with a CMOS camera (*Omron Senntech Co*, Japan). Sequences were recorded at 300 frames/s and treated using Dyva software (*Alliance Vision*, France).

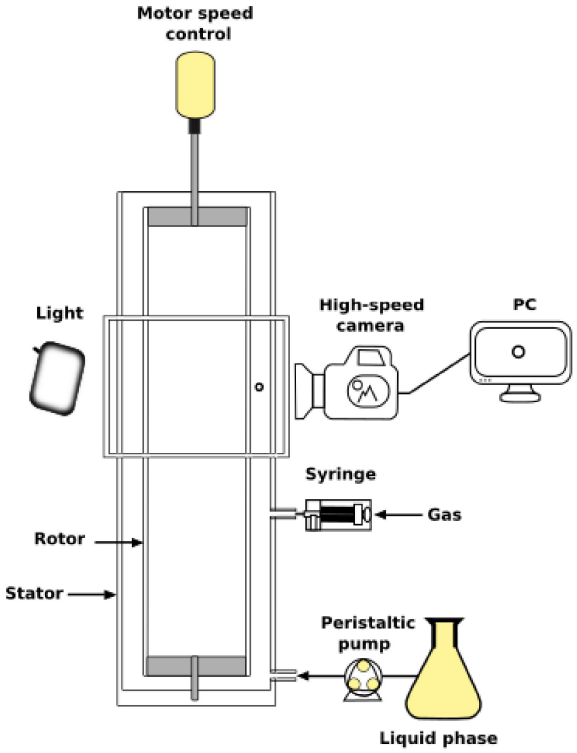

Figure 2: Illustration of the transparent Couette system: side view.

Images of undeformed bubbles were realized to determine the initial bubble diameter, which remained between 300 and 900 µm, ($0.15e_{Couette}$ to $0.45e_{Couette}$) in order to prevent border effect due to the cylinder walls. Next the video recordings were realized at different rotation speeds to analyze bubble deformation and determine the minimum value of shear rate needed to achieve break-up with a given bubble size. Shear rate $\dot{\gamma}$ is estimated by the Couette approximation where R_i is the radius of the inner cylinder and N its rotation speed:

$$\dot{\gamma} = \frac{2\,\pi\,R_i\,N}{e_{couette}} \tag{10}$$

In a second time, to better understand the nature of bubble division, the internal cylinder was replaced by a transparent impeller, close to that of NAGU, but of 35 mm diameter, so that the maximum shear rate was still provided by Eq. (10), but with flow conditions closer to aeration process.

3. RESULTS

3.1. Foaming performances in the stainless steel NAGU

Fig. 3 displays *foaming efficiency* for each SAA model-solution in 1- and 3-stage NAGU. It emerges that WPC solution was the only one reaching full gas incorporation from 200 to 1200 rpm, with only 1-stage column. Consequently, no significant effect of rotation speed was observed with this SAA. When replacing WPC with SCN, foaming efficiency reached at most 55% (N=1200 rpm) with the 1-stage column, while *foaming efficiency* increased to 89% (N=1200 rpm) at 3-stage column;

in both cases, efficiency was independent of *N*. This increase suggests that one could achieve full gas incorporation by further increasing the foam residence time in the column, i.e., by reducing gas and liquid flow rates or adding an additional stage. With TW20 as SAA, maximum foaming efficiency reached 80% at 800 rpm for 1-stage column; this value decreased with increasing *N* and reached 28% at 1200 rpm. When the whole column was used (three stages), foaming efficiency was improved and reached 98% at 200 rpm; but this value decreased when *N* was increased and reached 39% at 1200 rpm. Rotation speed increase acted as a centrifugation effect promoting phase separation and/or coalescence of large bubbles instead of enhancing foam formation, as shear and elongation forces increase with *N*. Similar observation had also been reported with Tween 80 [Narchi et al., 2007], another LMW surfactant structurally close to Tween 20. It clearly appears from these results that both SAA families (protein and LMW surfactant) act differently regarding gas dispersion even using the same operating conditions.

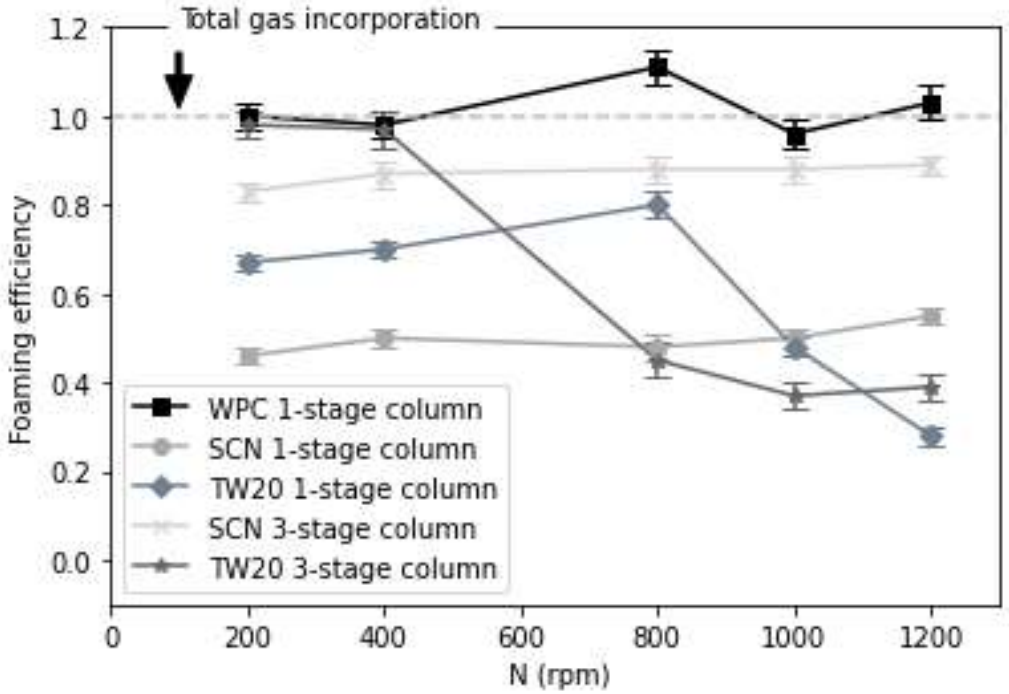

Figure 3: Foaming efficiency as a function of the rotation speed for WPC, SCN, and TW20. Experiments carried out with NAGU.

A comparison of bubble sizes as a function of rotation speed is displayed in Table 3. With the reference residence time (1-stage column), SCN- and TW20-stabilized bubbles were bigger than those stabilized by WPC. Mean diameter was nearly the same, whatever the rotation speed for WPC, whereas bubble size decreased when *N* increased with SCN and TW20 solutions. This latter trend had been widely reported in the literature for different foaming devices [Jabarkhyl et al., 2020; Badve, 2020; Mary et al., 2013]. Increasing *N* resulted in higher shear stress inside the column, inducing the break-up of larger bubbles into smaller ones, but it also led to more uniform and narrower bubble size distribution (data not shown). When residence time was increased by adding two more stages, SCN- and TW20-stabilized bubble size were close to those of bubbles stabilized by WPC at 1-column stage (10-20 µm), which seems to be the minimum size achievable with this device. The sensitivity to the increase in *N* became much less important than at 1-stage column. Regarding standard deviation, it also decreased considerably for SCN and TW20.

Table 3: Bubble mean diameter (D_{mean}) and standard deviation (SD). Experiments performed with NAGU at 1- and 3-stage column.

N (rpm)	$D_{mean} \pm$ SD (µm) 1-stage column ($\bar{t} = 188\ s$)			$D_{mean} \pm$ SD (µm) 3-stage column ($\bar{t} = 564\ s$)	
	WPC	SCN	TW20	SCN	TW20
200	17 ± 4	50 ± 30	50 ± 40	15 ± 6	20 ± 9
400	17 ± 4	50 ± 20	50 ± 40	13 ± 4	19 ± 7
800	17 ± 4	40 ± 20	40 ± 20	11 ± 3	16 ± 5
1000	15 ± 4	40 ± 20	40 ± 20	11 ± 3	14 ± 7
1200	14 ± 3	30 ± 10	30 ± 20	12 ± 4	13 ± 6

This latter result is confirmed by observing bubble size distribution (BSD) reported in Fig. 4. A unimodal profile was observed at 1-stage column with WPC. BSD was larger and rather bimodal with SCN and TW20 solutions. When residence time was increased (Fig. 4b), BSD became nearly unimodal for SCN and TW20, which was also consistent with the reduction in the standard deviation. It must be mentioned that BSD for foams stabilized by SCN and TW20 only includes bubbles successfully dispersed within the foaming device, while big gas plugs observed when the efficiency was less than 1 were excluded. A conclusion can be that if primary bubbles started to be split, they could be reduced by serial break-up to small bubbles, especially with longer residence times, whereas bubbles that did not undergo dispersion formed gas pockets.

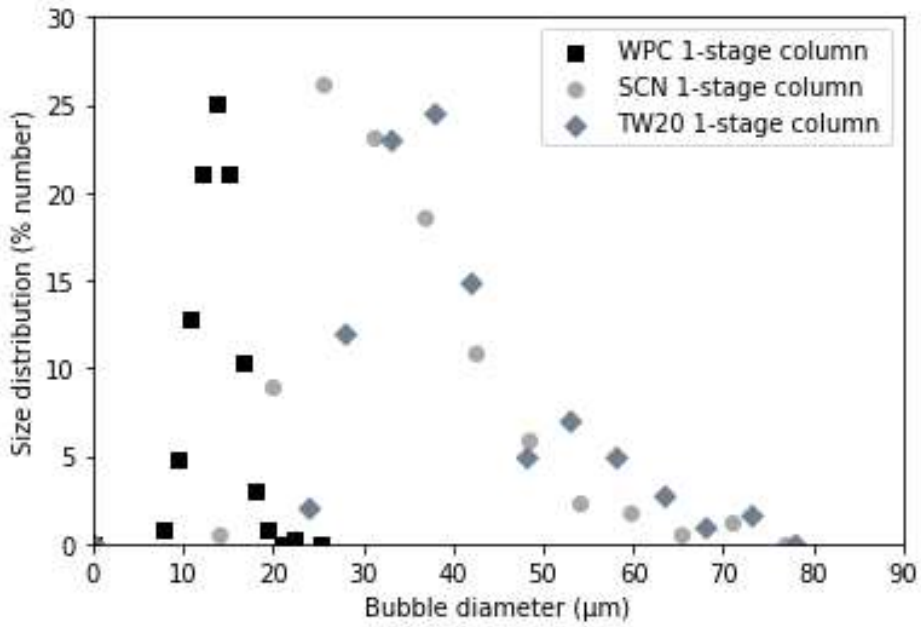

(a)

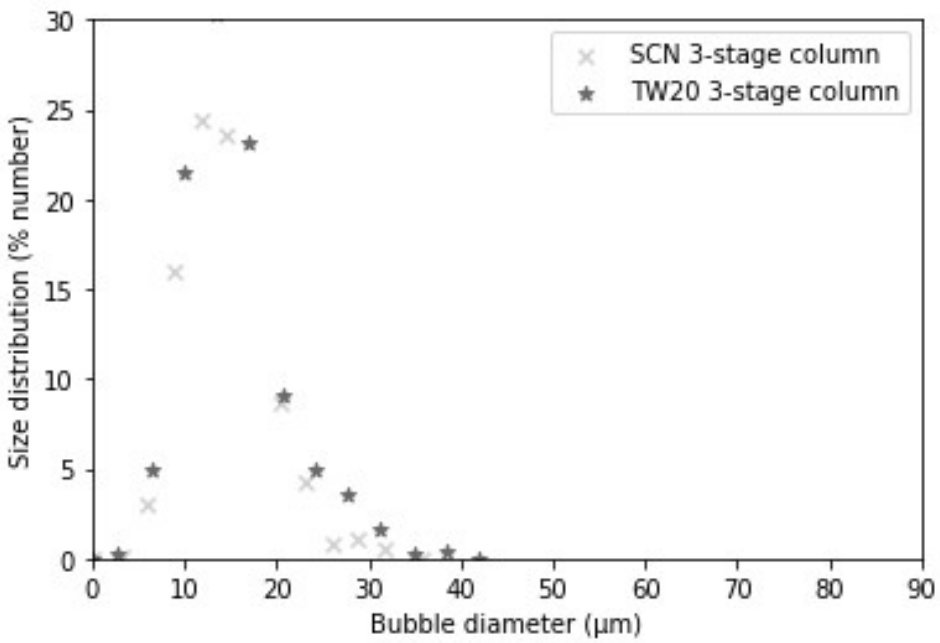

(b)

Figure 4: Effect of surface-active agents on bubble size distribution. Results for N = 1200 rpm in (a) 1 and (b) 3-stage column.

3.2. Foaming performance in the RS

To confirm the results obtained with the NAGU device, the residence time's effect was also studied on foaming operation using the RS device. Aeration was first carried out with the flow rates G_i = 10 and L_i = 30 mL/min. WPC solution reached maximum efficiency, whatever N, while SCN solution achieved at most 90% efficiency (Fig. 5). Increase in residence time by a factor 3 led to a total gas incorporation with the SCN solution. This differed from the NAGU device for which this residence time increase was not high enough to incorporate all the gas. This could be explained by the fact that the residence time with the RS at flow rates G_i = 3.3 and L_i = 10 mL was greater than with the NAGU at flow rates G_i = 10 and L_i = 30 mL (Table 2). As with NAGU, the efficiency seems independent of N in RS with SCN and WPC solutions. With the TW20 solution for the smallest residence time, 100% efficiency was achieved at 200 rpm; then, it decreased when increasing N down to 23% at 1200 rpm. In addition, increase in residence time did not lead to a better foaming efficiency, and this rise did not change the sensitivity of foaming efficiency to the increase in N. It can be deduced that this negative dependence of *foaming efficiency* on N seems to be a characteristic of TW20 solution, which is consistent with the observations and conclusions obtained in NAGU experiments.

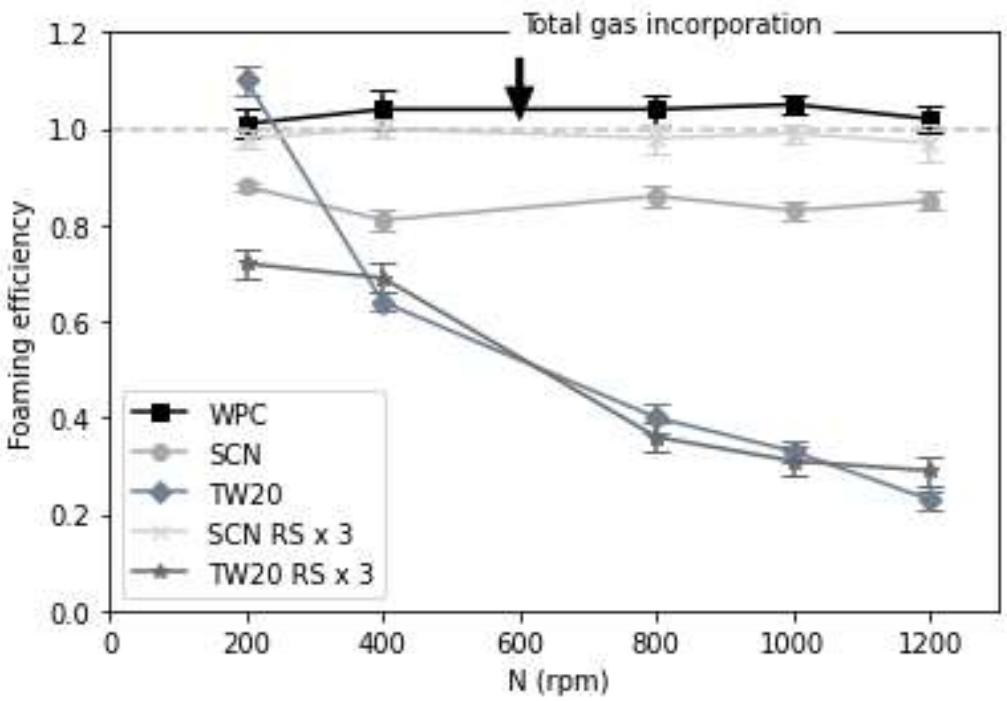

Figure 5: Foaming efficiency as function of the rotation speed. Experiments carried out with RS. "RS x 3" denotes the residence time's increase by 3 times (G_i = 3.3 and L_i = 10 mL/min).

Regarding bubble size and BSD, Table 4 shows that the RS device produced bigger bubbles than the NAGU, especially at low rotation speed. This difference decreased as N increased. Bubbles reached their minimum diameter when N exceeded a threshold speed which was around 800-1000 rpm. It should be pointed out that the axial distance available for the fluids (gap) is smaller in the NAGU (1 mm) than in the RS (2.5 mm). Therefore, the maximum shear rate is greater in the NAGU than in the RS; this explains why the NAGU allowed obtaining smaller bubbles than the RS especially for WPC. Residence time increase from 270 s to 812 s allowed a reduction in bubble size whatever the SAA (Table 4). This impact was significant at low rotation speed, but almost insignificant above 800 rpm.

Table 4: Bubble mean diameter (D_{mean}) and standard deviation (SD). Experiments performed with the RS device, with $\bar{t}$ = 270 s and $\bar{t}$ = 812 s.

N (rpm)	D_{mean} ± SD (µm) $\bar{t}$ = 270 s			D_{mean} ± SD (µm) $\bar{t}$ = 812 s	
	WPC	SCN	TW20	SCN	TW20
200	50 ± 20	50 ± 20	90 ± 80	27 ± 8	30 ± 20
400	40 ± 20	21 ± 7	50 ± 20	20 ± 8	30 ± 10
800	40 ± 20	14 ± 5	30 ± 20	16 ± 5	21 ± 9
1000	40 ± 10	14 ± 5	30 ± 20	15 ± 5	22 ± 9
1200	28 ± 7	14 ± 4	20 ± 20	14 ± 5	22 ± 9

3.3. Single bubble deformation and break-up

Bubble deformation and break-up were observed in the transparent Couette device. The three same SAA solutions (WPC, SCN, and TW20) were used for this study. During the experiments, air bubbles were generated in the solutions, a steady shear was applied, and the deformation (D for $Ca < 1$ and L/a for $Ca > 1$) was calculated from image analysis. Fig. 6 shows the development of bubble deformation in simple shear flow in the transparent Couette device. For each SAA, the first frame displays an initial bubble without shear stress: bubbles were thus assumed to be spherical in shape. Under the action of a constant shear flow, these bubbles initially at rest immersed in the model solution progressively deformed; after a transient time, it reached a steady state as long as conditions remained the same (Fig. 6 from frame 2). Regardless of the SAA used, raising shear rate induced an increase in deformation.

For protein-stabilized bubbles, deformation increase led to a break-up by *tip-streaming* (Fig. 6 frame 3 for WPC and SCN). This is a break-up mode in which a stream of tiny bubbles is ruptured off the tips of the bubble. This mode takes place randomly on the front or at the back of the bubble. At this stage, shear rate value was determined and used to calculate the critical Capillary number Ca_c from Eq.1. Observations also showed that beyond Ca_c, a filament appeared on both sides of the bubble, and the higher the shear rate, the longer this filament. This eventually led to a serial break-up and the release of tiny bubbles in a *jetting mode* (Fig. 6 frame 4 for WPC and SCN) as observed in microfluidic systems [Montanero and Gañán-Calvo, 2020]. In addition, the releasing frequency of daughter-bubbles with this break-up mode was higher than in the case of a simple *tip-streaming* and the released-bubbles were smaller.

Like bubbles stabilized by proteins, as the shear rate was increased, TW20-stabilized bubbles became thinner and longer. However, shear rate values which led to the rupture of bubbles stabilized by proteins did not induce break-up with TW20-stabilized bubbles. They continued deforming and lengthening as shear rate increased (Fig. 6 frame 2-4 for TW20).

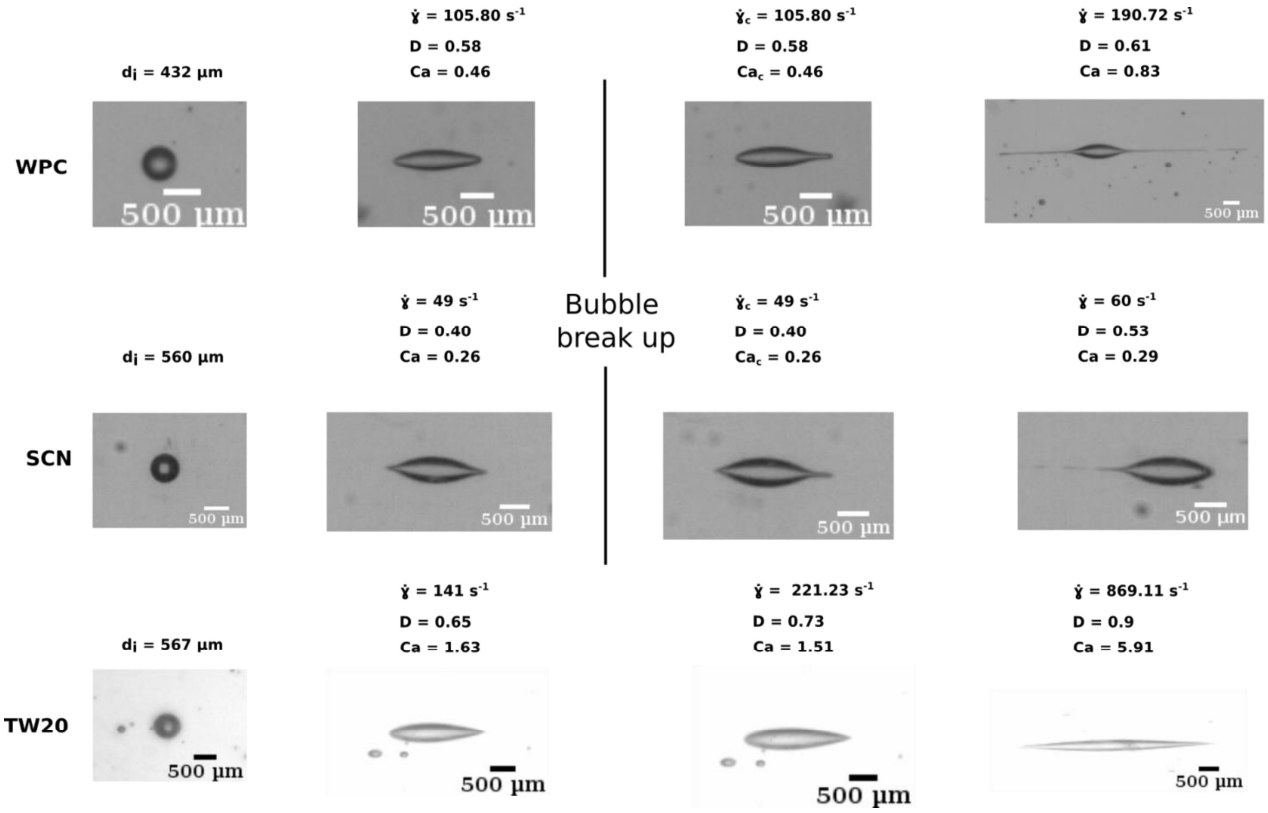

Figure 6: Air bubble initial shape, then deformed, and break-up (only for protein-stabilized bubbles) in simple shear flow (Couette device, scale on each frame). The applied shear rate is increased from the left to right (frame 1 to frame 4). The viscosity ratio λ is between $1.68.10^{-5}$ and $2.20.10^{-5}$, and the scale's marks on each frame corresponds to 500 µm.

As described, qualitative analysis with the proteins (WPC and SCN) showed similar bubbles behaviors. However, significant differences were observed in quantitative data. To examine the relationships between bubble deformation and Capillary number, bubble deformation parameter D of the bubbles vs. Ca was plotted on Fig. 7a. Experimental data displayed that for $Ca \leq 0.5$, D scaled with Ca, and bubbles were nearly spherical. This relationship was first observed with droplets by Taylor [1934] for small deformations ($Ca << 1$). Furthermore, as shown in Fig. 7a, SCN-stabilized bubbles deformed more than WPC-stabilized bubbles, leading to a smaller critical Capillary number Ca_c. In fact, bubbles stabilized with SCN broke for $Ca = 0.27$, while those stabilized with WPC broke for $Ca = 0.5$. Above these values, D remained constant around 0.5-0.6.

Regarding bubbles stabilized by TW20 for $Ca < 1$ (Fig. 7a), they deformed less than protein-stabilized bubbles, and in the end, as said before, they did not break. To reach the same deformation degree as bubbles stabilized by proteins, Ca values higher than 1 were necessary. For Ca values from 1 to 5, D increased from 0.6 to 0.9 (data not shown). At these high deformations ($Ca > 1$) the parameter L/a is commonly used to describe the deformation degree. Fig. 7b presents a plot of this parameter as a function of Ca. Experimental results are compared to the theoretical predictions of Hinch and Acrivos [1979] (Eq.4) and to the experimental results of Canedo et al. [1993] (Eq.5). Power law models (Eq. 3) fitting the data were reported in the figure for the three cases. For TW20 solution, experimental data seems to follow the same trend of the literature. The values of the constant α appear to be in the same order of magnitude, while those of β differ slightly. Remarkably, experimental results are close to those of Canedo et al. [1993] where SAA were not used, but the equilibrium

surface tension of their solution was around 33-41, notably close to that of TW20 solution, as if this parameter was important regarding large deformation.

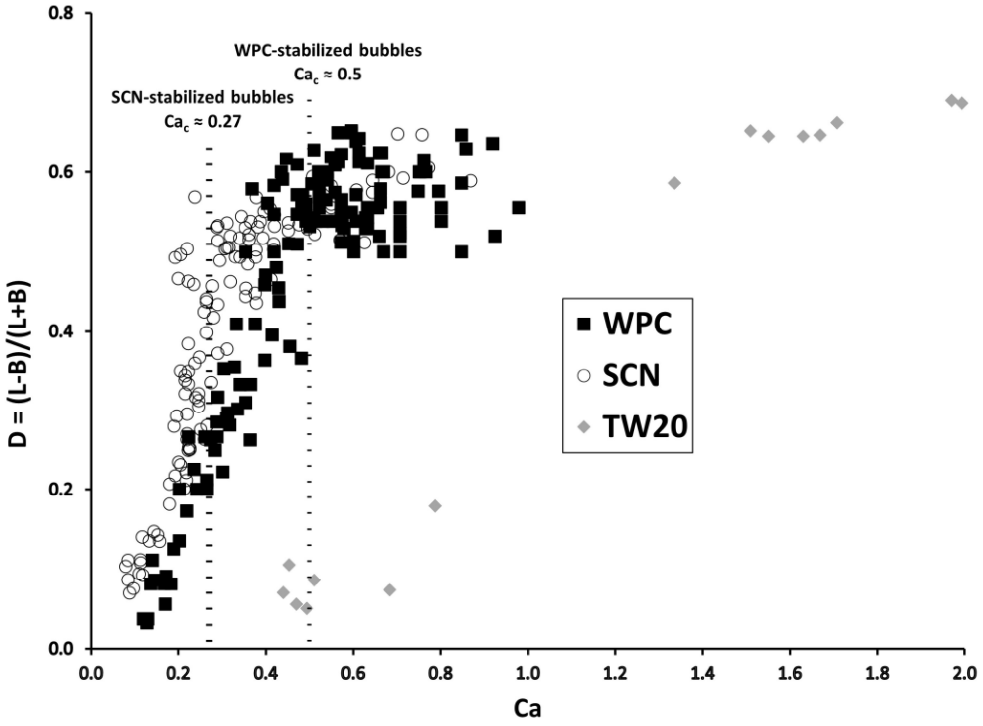

(a)

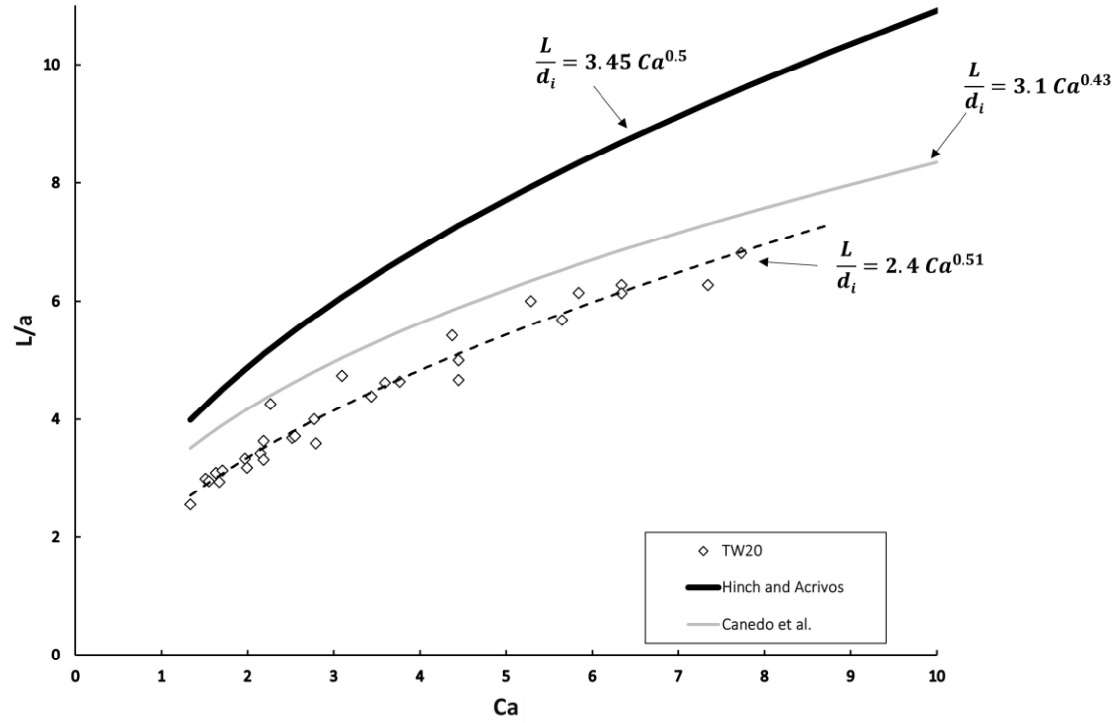

(b)

Figure 7: (a) Deformation parameter D as a function of the Capillary number Ca for bubbles stabilized by proteins and surfactant agents in simple shear flow; (b) Deformation parameter L/a as a function of the Capillary number Ca for bubbles stabilized by Tween 20 in simple shear flow. Symbols represent measured values, and the dashed line is to guide the eye. The solid thick line is the prediction by Hinch and Acrivos [1979] based on slender body theory. The thin grey line refers to the model prediction by Canedo et al. [1993].

Even though the TW20 model-solution did not allow a full gas incorporation in aeration process, a fraction of the gas was incorporated; this means that bubble break-up took place in the apparatus anyway. To better understand the nature of bubble division, the Couette device internal cylinder was replaced by a transparent impeller. This setup was used to analyze qualitatively bubble break-up phenomena in dispersion conditions with WPC, SCN, and TW20 solutions (Fig. 8). Under the same operating conditions, break-up by the bubble tip with a single or multiple daughter bubble seemed to be the main break-up mode for bubbles stabilized by WPC (Fig. 8a), and this confirms the results obtained previously. The same observation was made with SCN (data not shown). Using TW20 as SAA, either no break-up was observed as in the Couette device, or a new break-up mode appeared. It was a total break-up in which the central part of the bubble formed a neck in the middle that progressively thinned, and finally, the bubble splits into two main daughter-bubbles in a binary break-up mode, forming also small satellite bubbles in between (Fig. 8b). This break-up mode had already been reported in microfluidic systems with junctions [Fu et al., 2011]. It was also observed in the foaming device (NAGU) between two successive mixing elements. Actually, bubbles were torn between two depression areas at the back of the paddles in a Venturi effect. In this case, break-up was not a consequence of pure shear but rather of an elongational flow.

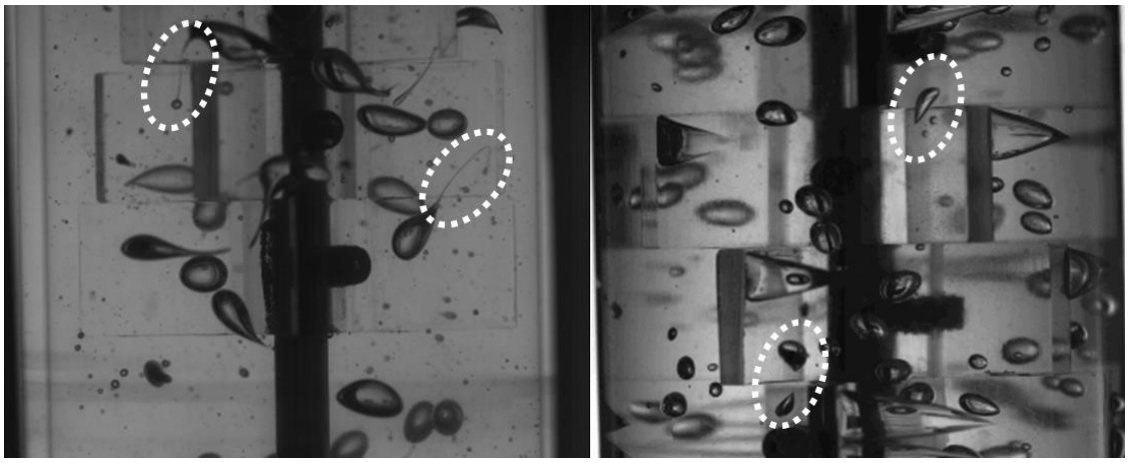

(a) *(b)*

Figure 8: Bubble break-up mechanism (white dashed line) under given rotational speed (200 rpm): (a) tip-break-up with WPC and (b) absence or total break-up with TW20.

These results highlight the qualitative and quantitative differences between the three SAA at bubble scale. The observed differences are related to the break-up threshold, but also to the break-up mode, and they can be a way to better understand the pilot-scale results.

4. DISCUSSION

In the previous section, experimental results indicated that: (1) foam production was more efficient with WPC compared to SCN and TW20; (2) bubbles coated by WPC and SCN broke by *tip-streaming* at low shear rate and a smaller *Ca* was required for SCN-stabilized bubbles than for those stabilized by WPC; (3) TW20-stabilized bubbles did not break even at higher shear rate or broke by the binary break-up mode. These results underline the differences in the behavior of SAA at the bubble interface leading to a different foaming result. Souidi et al. [2012] already tried to establish a direct link between a single bubble break-up experiment and pilot-scale foaming results with WPI (whey protein isolate). Since *tip-streaming* requires a lower shear rate [Grace, 1982], bubble rupture was facilitated by this mode, and BSD was narrower. This observation can be extended to SCN even though break-up thresholds were different. On the other hand, the lack of tip-break-up with TW20 seems to lead to poor foaming results.

As shown in Table 1, the SAA's nature strongly influences the equilibrium surface tension (σ_{sc} = 55.4, σ_{WPC} = 50.4, and σ_{TW20} = 35.2 mN/m). Even though TW20 allowed a greater reduction in equilibrium surface tension than proteins, it did not enhance gas dispersion compared to proteins, as it can be deduced from the pilot-scale results. Thus, considering only the absolute value of equilibrium surface tension (σ) is not consistent with the break-up processes once a bubble is submitted to shear flow. Moreover, the three solutions almost had the same viscosity and experiments were performed under the same operating conditions. Therefore, the absence (TW20) or presence (WPC, SCN) of tip-break-up phenomena could not only be attributed to the laminar flow and/or to the low viscosity ratio, but likely to the way these SAA stabilized interfaces. It is then more relevant to consider the local and/or dynamic surface tension which is influenced by the SAA surface coverage during foam formation.

Tip-streaming was mainly attributed to an interfacial tension gradient due to the presence of surfactants, resulting in reduced interfacial tension at the tips as proposed by de Bruijn [1993] and Eggleton et al. [1999] who worked on drops. In the case of bubbles, to reach this surface tension gradient, the surfactants must (*i*) migrate from the bulk to the interface, (*ii*) adsorb to the interface, and (*iii*) convey during deformation towards the bubble ends, which results in large tip stretching.

LMW emulsifiers, such as TW20, stabilize bubbles in the short range through the Gibbs–Marangoni mechanism acting in the tangential direction and opposite to the direction in which the surfactants are pushed by the flow [Moyle et al., 2012]. In fact, bubbles are stabilized by a mobile monomolecular layer with low surface viscoelasticity, in which rapid diffusion within the surface layer and exchange with the bulk solution occur [Mackie and Wilde; 2005]. This relies on the surfactants which rapidly migrate to regions of the interface depleted of surfactant because of deformation. This could be an explanation for the different deformation behaviors observed with proteins (SCN and WPC) and TW20: TW20 seems to have a better ability to migrate and adsorb at the interface than proteins, preventing the accumulation at the tips even at a very high shear rate. It should also be mentioned that although the mass percent of SAA in the solutions is the same (2%), the number of molecules in the solutions is not equivalent due to the structural and molecular weight differences of these two SAA families. In addition, Miller et al. [2005] reported that proteins desorption rate, such as *β-lactoglobulin* and *β-casein*, is 10^4 to 10^8 times slower than that of conventional surfactants. Therefore, desorption in the case of TW20 could also limit the SAA concentration gradient. The matter comes down to the comparison between two characteristic times: the first is the SAA accumulation's time at the tips induced by shear stress; the second is the migration

time either from the bulk to the free interface created or the desorption time from the interface. Considering the differences between TW20 and proteins, these characteristic times should be shorter for TW20. Moreover, with surfactants, the Marangoni effect could also curb the deformation. Consequently, much higher shear stress would be required with TW20 to get tip-break-up in shear flow [Abbassi-Sourki et *al*., 2012]. An approximate value for this shear rate could be calculated using the results from Grace [1982] on droplets in simple shear flow. The extrapolation suggests that bubbles should break by binary break-up mode for $Ca_c \approx 60$ when $\lambda = 2.2\ 10^{-5}$, corresponding to a shear rate around 2400 s^{-1}. As shown in Table 2, this value is out of reach with the devices used for aeration and, nonetheless, bubble mean diameter (Table 3 and 4) is slightly superior with TW20 compared to proteins, suggesting the occurrence of break-up. As Grace's work [1982] involved droplets and not bubbles, the calculated shear rate value (2400 s^{-1}) is probably overestimated. In addition, Ca_c proposed by Grace [1982] at a low viscosity ratio was not obtained for tip-break-up. In this study, tip-break-up was also likely to occur with TW20 at a rather high shear rate, but other break-up phenomena requiring lower power input may also occur, as observed in Fig. 8. As was simulated by Mardaru et al. [2012] with the NAGU device and by Wu et al. [2014] with a RS device, flows generated by aeration devices are complex, offering the possibilities for various break-up modes, so that, rupture by tip-break-up does not seem to be the prevailing break-up mode with TW20, in contrast to WPC and SCN.

Bubbles stabilized by WPC and SCN broke by *tip-streaming*, which led to the formation of small bubbles with a narrow BSD, as observed during aeration operations with protein solutions. There is, however, an important matter to discuss: is tip-break-up at low shear rate specific to the presence of HMW surfactants such as proteins? According to de Bruijn [1993], *tip-streaming* neither occurs at extremely low surfactant concentration, nor at high level where bubble coverage by surfactant is guaranteed. But in the Couette device experiments, the second condition is fulfilled (2% w/w) and this rupture mode was, nevertheless observed. In addition, Müller-Fischer et al. [2008] observed bubble break-up by *tip-streaming* in glucose syrup solutions without any SAA and concluded that tip-break-up occurred preferentially for bubbles even if there was no surface tension gradient. All this data supports the idea that the understanding of bubble break-up mechanisms is far from complete, but the present results tend to associate the use of proteins under laminar conditions in food aeration to *tip-streaming*.

Regarding the break-up threshold, SCN- and WPC-stabilized bubbles broke around $Ca_c \approx 0.27$, and $Ca_c \approx 0.5$, respectively. This difference in threshold could be explained by the viscoelasticity of the layers formed around bubbles by these different protein types. The viscoelastic character of the films formed by sodium caseinates, and whey proteins was analyzed in the literature: it appears that the viscoelasticity of caseinate-adsorbed films was lower than that of WPC-adsorbed films [Cicuta, 2007; Álvarez Gómez and Patino, 2007]. According to these papers, interfacial layers formed by globular proteins tend to be more viscoelastic than those formed by flexible, random-coil proteins, such as β-casein. Then, the higher viscoelastic character of WPC-adsorbed layers seems to make bubble surface less prone to deformation and rupture under shear stresses, which agrees with the higher value of Ca_c obtained with WPC compared to SCN. It could, thus, be expected a better foaming efficiency at pilot-scale with SCN but the contrary was observed. How could this be explained? Efficiency and final BSD obtained after a foaming process is a result of a dynamic equilibrium between bubble break-up and coalescence phenomena [Séguineau de Préval et al., 2014]. The question is, therefore, to know whether SCN-stabilized bubbles were subjected to coalescence

phenomena. Due to the geometry of the aeration devices used, observing coalescence dynamics inside the devices was not possible. There is, nonetheless, one argument against the coalescence hypothesis: with SCN solution, foaming efficiency was raised to 100% by increasing residence time. That does not mean that coalescence was absent in these experiments but in the context of aerated food with ε=25%, contact between bubbles is limited. Another reason could justify why SCN did not achieve maximum efficiency during aeration: bubble surface coverage. During the visualization of single bubble deformation, SCN concentration (2% w/w) was not a limitation to bubble break-up at low *Ca* since only few bubbles were generated in a large amount of solution (ε<1%). Therefore, there were enough available SAA's molecules to cover the bubble surface and achieve bubble break-up. In the case of aeration, surface area was increased by gas incorporation under mechanical stirring. As a result, the amount of protein molecules needed to cover the bubble surface raised steeply at pilot scale. If this protein amount is locally not sufficient, it may impact bubble deformation and break-up mechanisms. The problem, however, is not only related to the number of molecules needed at air/water interface, but also to the time necessary for them to migrate from the bulk to the interface by diffusional transport. A higher residence time led, thus, to a better casein molecule availability, so that, increase in residence time could induce a total gas incorporation using RS, even if it meant a slower production rate.

5. CONCLUSION

A comparative experimental study dealing with food aeration at pilot scale and the visualization of bubble deformation and break-up with three different SAA was conducted. The air/water interface behaviors strongly depended on SAA when submitted to shear flows. Proteins, as HMW SAA, promoted tip-streaming as the major break-up phenomenon due to local surface tension gradients. Break-up thresholds differed between proteins because they acted differently at air/water interface. TW20 as a LMW SAA, on the other hand, did not favor bubble break-up by simple shear flow and needed either high shear or more complex flows to split bubbles. These observations provided interesting insights to understand the macroscopic results on food aeration but could not explain the kinetically governed differences reported between proteins.

Gathering information on the way surface-active agents migrate towards and adsorb dynamically to bubbles surface, coupled to bubble deformation and break-up visualization under different types of flows seems, therefore, a promising approach to better understand foam generation and to reach the long-term goal of predicting the achievement of aeration operations.

Funding

This research did not receive any specific grant from funding agencies in the commercial, or not-for-profit sectors.

CRediT authorship contribution statement

Boubakar Sanogo: Investigation, Formal Analysis, Software, Data analysis, Writing - original draft. **Kaies Souidi**: Investigation, Formal Analysis, Software, Data analysis. **Alain Marcati**: Conceptualization, Methodology, Validation, Supervision, Writing - review & editing. **Christophe Vial**: Conceptualization, Methodology, Validation, Supervision, Writing - review & editing.

Declaration of Competing Interest

The authors declare that they have no known competing financial interests or personal relationships that could have appeared to influence the work reported in this paper.

References

Abbassi-Sourki, F., Bousmina, M., Huneault, M. A. (2012). Effect of interfacial modifier on single drop deformation and breakup in step increasing shear flow. *Rheol. Acta*, 51, 111-126. https://doi:10.1007/s00397-011-0602-x.

Álvarez Gómez, J. M., Rodríguez Patino, J. M. (2007). Viscoelastic Properties of Diglycerol Ester and Protein Adsorbed Films at the Air−Water Interface. *Ind. Eng. Chem. Res.*, 46, 2693-2701. https://doi:10.1021/ie061451g.

Badve, M. (2021). A novel gas inducing rotor-stator impeller for gas-liquid foam generation. *Chemical Engineering and Processing - Process Intensification*, 159, 108216. https://doi:10.1016/j.cep.2020.108216.

Bezelgues, J. -B., Serieye, S., Crosset-Perrotin, L., Leser, M. E. (2008). Interfacial and foaming properties of some food grade low molecular weight surfactants. *Colloids and Surfaces A: Physicochemical and Engineering Aspects*, 331, 56-62. https://doi:10.1016/j.colsurfa.2008.07.022.

Bykov, A.G., Liggieri, L., Noskov, B.A., Pandolfini, P., Ravera, F., Loglio, G. (2015). Surface dilational rheological properties in the nonlinear domain. *Advances in Colloid and Interface Science*, 222, 110-118. https://doi.org/10.1016/j.cis.2014.07.006.

Canedo, E. L., Favelukis, M., Tadmor, Z., Talmon, Y. (1993). An experimental study of bubble deformation in viscous liquids in simple shear flow. *AIChE J.*, 39, 553-559. https://doi:10.1002/aic.690390403.

Cantat, I., Cohen-Addad, S., Elias, F., Graner, F., Höhler, R., Pitois, O., Rouyer, F., Saint-Jalmes, A. (2013). Uses of foams. In: Oxford University Press (Eds.), *Foams: Structure and Dynamics* (pp. 1-16). https://doi.org/10.1093/acprof:oso/9780199662890.003.0001.

Cicuta, P. (2007). Compression and shear surface rheology in spread layers of β-casein and β-lactoglobulin. *Journal of Colloid and Interface Science*, 308, 93-99. https://doi:10.1016/j.jcis.2006.12.056.

De Bruijn, R. A. (1993). Tipstreaming of drops in simple shear flows. *Chemical Engineering Science*, 48(2), 277-284. https://doi.org/10.1016/0009-2509(93)80015-I.

Eggleton, C. D., Pawar, Y. P., Stebe, K. J. (1999). Insoluble surfactants on a drop in an extensional flow: a generalization of the stagnated surface limit to deforming interfaces. *Journal of Fluid Mechanics*, 385, 79-99. https://doi:10.1017/S0022112098004054.

Einhorn-Stoll, U., Weiss, M., Kunzek, H. (2002). Influence of the emulsion components and preparation method on the laboratory-scale preparation of o/w emulsions containing different types of dispersed phases and/or emulsifiers. *Nahrung/Food*, 46, 294-301. https://doi:10.1002/1521-3803(20020701)46:4<294::AID-FOOD294>3.0.CO;2-2.

761 Fox, Patrick F., Guinee, Timothy P., Cogan, Timothy M., McSweeney Paul L. H. (2017). Chemistry
762 of Milk Constituents. In: Springer (Eds.), *Fundamentals of Cheese Science* (pp. 71-104). E-
763 Publishing Inc. https://doi.org/10.1007/978-1-4899-7681-94.

764 T. Fu, Y. Ma, D. Funfschilling, H.Z. Li (2011)**.** Dynamics of bubble breakup in a microfluidic T-
765 junction divergence**.** *Chemical Engineering Science***,** 66 (18)**,** 4184-
766 4195.https://doi.org/10.1016/j.ces.2011.06.003.
767
768 H. P. Grace (1982). Dispersion phenomena in high viscosity immiscible fluid systems and application
769 of static mixers as dispersion devices in such systems. *Chemical Engineering Communications*, 14,
770 225-277. https://doi.org/10.1080/00986448208911047.
771
772 E. J. Hinch, A. Acrivos (1980). Long slender drops in a simple shear flow. *J. Fluid Mech.*, 98,
773 305-328. https://doi:10.1017/S0022112080000171.
774
775 Thao Minh Ho, Aysan Razzaghi, Arun Ramachandran, Kirsi S. Mikkonen (2022). Emulsion
776 characterization via microfluidic devices: A review on interfacial tension and stability to coalescence.
777 *Advances in Colloid and Interface Science,* 299,102541. https://doi.org/10.1016/j.cis.2021.102541.
778
779 S. Jabarkhyl, M. Barigou, S. Zhu, P. Rayment, D. M. Lloyd, D. Rossetti (2020). Foams generated
780 from viscous non-Newtonian shear-thinning liquids in a continuous multi rotor-stator device.
781 *Innovative Food Science & Emerging Technologies*, 59, 102231.
782 https://doi:10.1016/j.ifset.2019.102231.
783
784 A. Mackie, P. Wilde (2005). The role of interactions in defining the structure of mixed protein–
785 surfactant interfaces. *Advances in Colloid and Interface Science*, 117, 3-13.
786 https://doi:10.1016/j.cis.2005.04.002.
787
788 A. Mardaru, K. Souidi, A. Marcati, G. Jinescu, C. Habchi, D. Della Valle, G. Djelveh (2012). Effect
789 of impellers configuration on the gas dispersion of high-viscosity fluid using Narrow Annular Gap
790 Unit. Part 2: numerical approach. *Chemical Engineering Science*, 75, 63-74.
791 https://doi:10.1016/j.ces.2012.02.056.
792
793 G. Mary, S. Mezdour, G. Delaplace, R. Lauhon, G. Cuvelier, et F. Ducept (2013). Modelling of the
794 continuous foaming operation by dimensional analysis. *Chemical Engineering Research and Design*,
795 91, 2579-2586. https://doi:10.1016/j.cherd.2013.05.020.
796
797 S. Mezdour, E. Séguineau de Préval, P. Granda, G. Cuvelier, F. Ducept (2017, March-April). Impact
798 of Interfacial Characteristics on Foam Structure: Study on Model Fluids and at Pilot Scale. *Oil Gas*
799 *Sci. Technol. – Rev. IFP Energies Nouvelles*, 72, Article 13. https://doi:10.2516/ogst/2017008.
800
801 R. Miller, D.O. Grigoriev, J. Krägel, A.V. Makievski, J. Maldonado-Valderrama, M. Leser, M.
802 Michel, V.B. Fainerman (2005). Experimental studies on the desorption of adsorbed proteins from
803 liquid interfaces. *Food Hydrocolloids*, 19, 479-483. https://doi:10.1016/j.foodhyd.2004.10.012.
804
805 J. M. Montanero, A. M. Gañán-Calvo (2020). Dripping, jetting and tip streaming. *Reports on*
806 *Progress in Physics*, 83. https://doi:10.1088/1361-6633/aba482.

T. M. Moyle, L. M. Walker, S. L. Anna (2012). Predicting conditions for microscale surfactant mediated tip-streaming. *Physics of Fluids*, 24, 082110. https://doi:10.1063/1.4746253.

N. Müller-Fischer, E. J. Windhab (2005). Influence of process parameters on microstructure of food foam whipped in a rotor-stator device within a wide static pressure range. *Colloids and Surfaces A: Physicochemical and Engineering Aspects*, 263, 353-362. https://doi:10.1016/j.colsurfa.2004.12.057.

N. Müller-Fischer, P. Tobler, M. Dressler, P. Fischer, E. J. Windhab (2008). Single bubble deformation and breakup in simple shear flow. *Exp. Fluids*, 45, 917-926. https://doi:10.1007/s00348-008-0509-1.

I. Narchi, C. Vial, M. Labbafi, G. Djelveh (2011). Comparative study of the design of continuous aeration equipment for the production of food foams. *Journal of Food Engineering*, 102, 105-114. https://doi:10.1016/j.jfoodeng.2010.07.030.

I. Narchi, C. Vial, G. Djelveh (2007). Influence of bulk and interfacial properties and operating conditions on continuous foaming operation applied to model media. *Food Research International*, 40, 1069-1079. https://doi:10.1016/j.foodres.2007.06.002.

J. M. Rallison (1981). A numerical study of the deformation and burst of a viscous drop in general shear flows. *J. Fluid Mech.,* 109, 465-482. https://doi:10.1017/S002211208100116X.

F. D. Rumscheidt, S. G. Mason (1961). Particle motions in sheared suspensions XII. Deformation and burst of fluid drops in shear and hyperbolic flow. *Journal of Colloid Science*, 16, 238-261. https://doi:10.1016/0095-8522(61)90003-4.

C. Rust, M. Manga (2002). Bubble Shapes and Orientations in Low Re Simple Shear Flow. *Journal of Colloid and Interface Science*, 249, 476-480. https://doi:10.1006/jcis.2002.8292.

S. Samanta, P. Ghosh (2011). Coalescence of bubbles and stability of foams in aqueous solutions of Tween surfactants. *Chemical Engineering Research and Design*, 89, 2344-2355. https://doi:10.1016/j.cherd.2011.04.006.

E. Séguineau de Préval, F. Ducept, G. Cuvelier, S. Mezdour (2014). Effect of bulk viscosity and surface tension kinetics on structure of foam generated at the pilot scale. *Food Hydrocolloids*, 34, 104-111. https://doi:10.1016/j.foodhyd.2012.12.001.

K. Souidi, A. Mardaru, M. Roudet, A. Marcati, D. Della Valle, G. Djelveh (2012). Effect of impellers configuration on the gas dispersion in high-viscosity fluid using narrow annular gap unit. Part 1: Experimental approach. *Chemical Engineering Science*, 74, 287-295. https://doi:10.1016/j.ces.2012.02.055.

Paul Stevenson (2012). *Foam engineering: fundamentals and applications* (1st Ed). Chichester, UK: John Wiley & Sons, Ltd. (Chapter 1).G. I. Taylor (1932). The viscosity of a fluid containing small drops of another fluid. *Proc. R. Soc. London A*, 138, 41-48. https://doi:10.1098/rspa.1932.0169.

G. I. Taylor (1934). The formation of emulsions in definable fields of flow. *Proc. R. Soc. London A*, 146, 501-523. https://doi:10.1098/rspa.1934.0169.

S. Torza (1971). R. G. Cox, S.G. Mason, Particle Motions in Sheared Suspensions XXVII. Transient Streamlines in and around liquid drops. *Journal of Colloid and Interface Science*, 35, 529-543. https://doi.org/10.1016/0021-9797(71)90211-6.

H. Wu, S. Shu, N. Yang, G. Lian, S. Zhu, M. Liu (2014). Modeling of power characteristics for multistage rotor–stator mixers of shear-thinning fluids. *Chemical Engineering Science*, 117, 173-182. https://doi:10.1016/j.ces.2014.06.039.

F. Zhan, M. Youssef, B. R. Shah, J. Li, B. Li (2022). Overview of foam system: Natural material-based foam, stabilization, characterization, and applications. *Food Hydrocolloids*, 125, 107435. https://doi:10.1016/j.foodhyd.2021.107435.

H. Zhang, G. Xu, T. Liu, L. Xu, Y. Zhou (2013). Foam and interfacial properties of Tween 20-bovine serum albumin systems. *Colloids and Surfaces A: Physicochemical and Engineering Aspects*, 416 23-31. https://doi:10.1016/j.colsurfa.2012.10.028.

Tables

Table 1: Physicochemical properties of the model-fluids.

SAA	Viscosity (Pa.s)	Surface tension (mN/m)	Density (kg/m^3)
WPC	1.1 ± 0.1	50.4 ± 0.3	1280 ± 10
SCN	0.92 ± 0.03	55.4 ± 0.3	1360 ± 10
TW20	0.84 ± 0.06	35.2 ± 0.2	1350 ± 30

Table 2: Main characteristics of the two foaming devices.

Parameters	NAGU	RS
Maximum shear rate $\dot{\gamma}_{max}$ (s^{-1}) at 1200 rpm*	2200	880
Volume mean shear rate $\dot{\gamma}_{mean}$ (s^{-1}) at 1200 rpm**	386	364
Residence time $(\bar{t})$ (s) - 1 stage; G_i/L_i = 10/30***	188	270
Residence time $(\bar{t})$ (s) - 3 stages; G_i/L_i = 10/30	564	-
Residence time $(\bar{t})$ (s) - 1 stage; G_i/L_i = 3.3/10	-	812

**Maximum shear rate is calculated with the Couette approximation*
***Volume mean shear rate is calculated with the Metzner and Otto approximation*
**** Residence time considered as the reference*

Table 3: Bubble mean diameter (D_{mean}) and standard deviation (SD). Experiments performed with NAGU at 1- and 3-stage column.

N (rpm)	D_{mean} ± SD (µm) 1-stage column ($\bar{t} = 188\ s$)			D_{mean} ± SD (µm) 3-stage column ($\bar{t} = 564\ s$)	
	WPC	SCN	TW20	SCN	TW20
200	17 ± 4	50 ± 30	50 ± 40	15 ± 6	20 ± 9
400	17 ± 4	50 ± 20	50 ± 40	13 ± 4	19 ± 7
800	17 ± 4	40 ± 20	40 ± 20	11 ± 3	16 ± 5
1000	15 ± 4	40 ± 20	40 ± 20	11 ± 3	14 ± 7
1200	14 ± 3	30 ± 10	30 ± 20	12 ± 4	13 ± 6

Table 4: Bubble mean diameter (D_{mean}) and standard deviation (SD). Experiments performed with the RS device, with $\bar{t}$ = 270 s and $\bar{t}$ = 812 s.

N (rpm)	D_{mean} ± SD (µm) $\bar{t} = 270\ s$			D_{mean} ± SD (µm) $\bar{t} = 812\ s$	
	WPC	SCN	TW20	SCN	TW20
200	50 ± 20	50 ± 20	90 ± 80	27 ± 8	30 ± 20
400	40 ± 20	21 ± 7	50 ± 20	20 ± 8	30 ± 10
800	40 ± 20	14 ± 5	30 ± 20	16 ± 5	21 ± 9
1000	40 ± 10	14 ± 5	30 ± 20	15 ± 5	22 ± 9
1200	28 ± 7	14 ± 4	20 ± 20	14 ± 5	22 ± 9

FIGURE 1A

Click here to access/download;Figure;FIGURE 1A.png

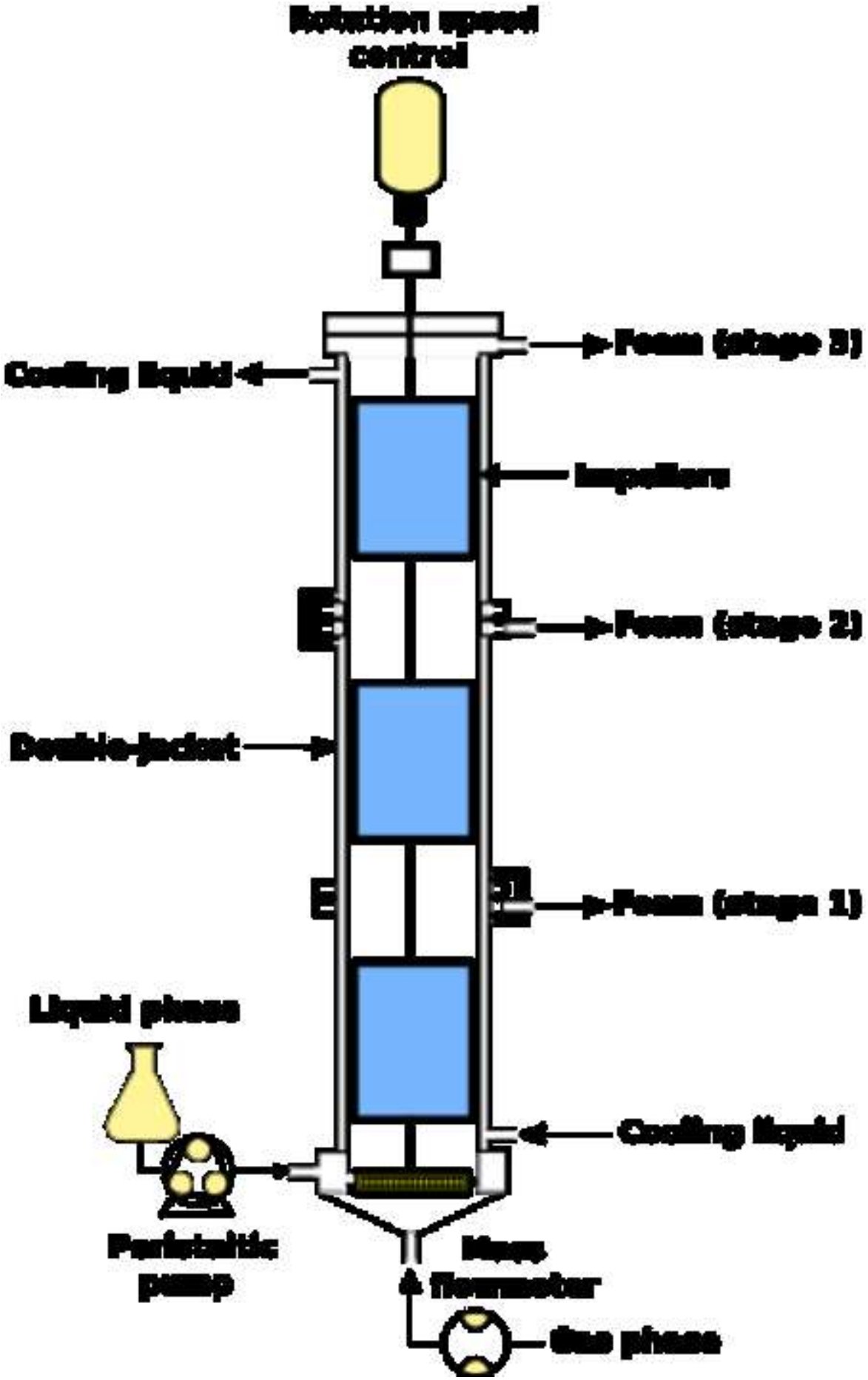

FIGURE 1B

Click here to access/download;Figure;FIGURE 1B.png

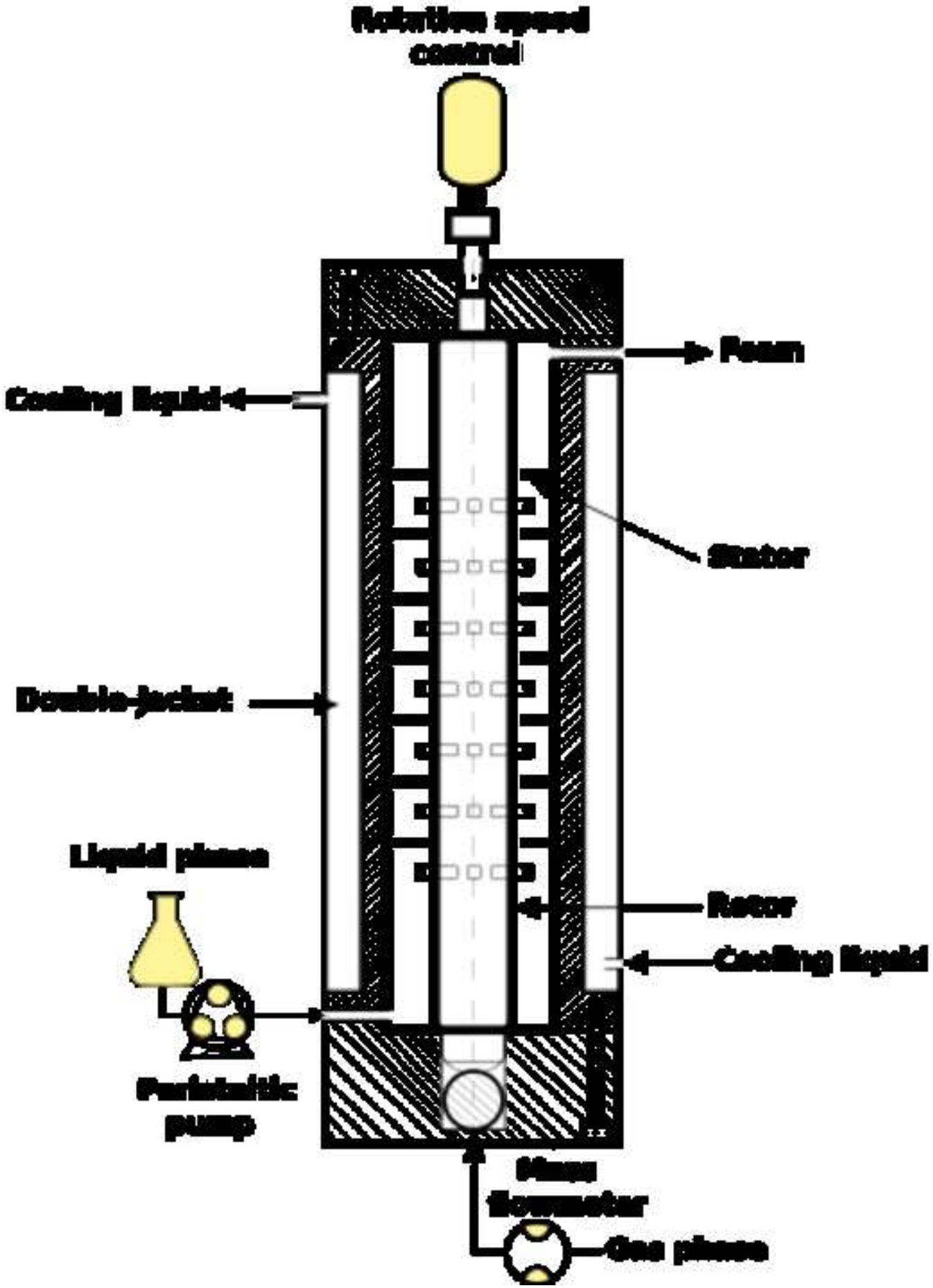

FIGURE 2

Click here to access/download;Figure;FIGURE 2.png

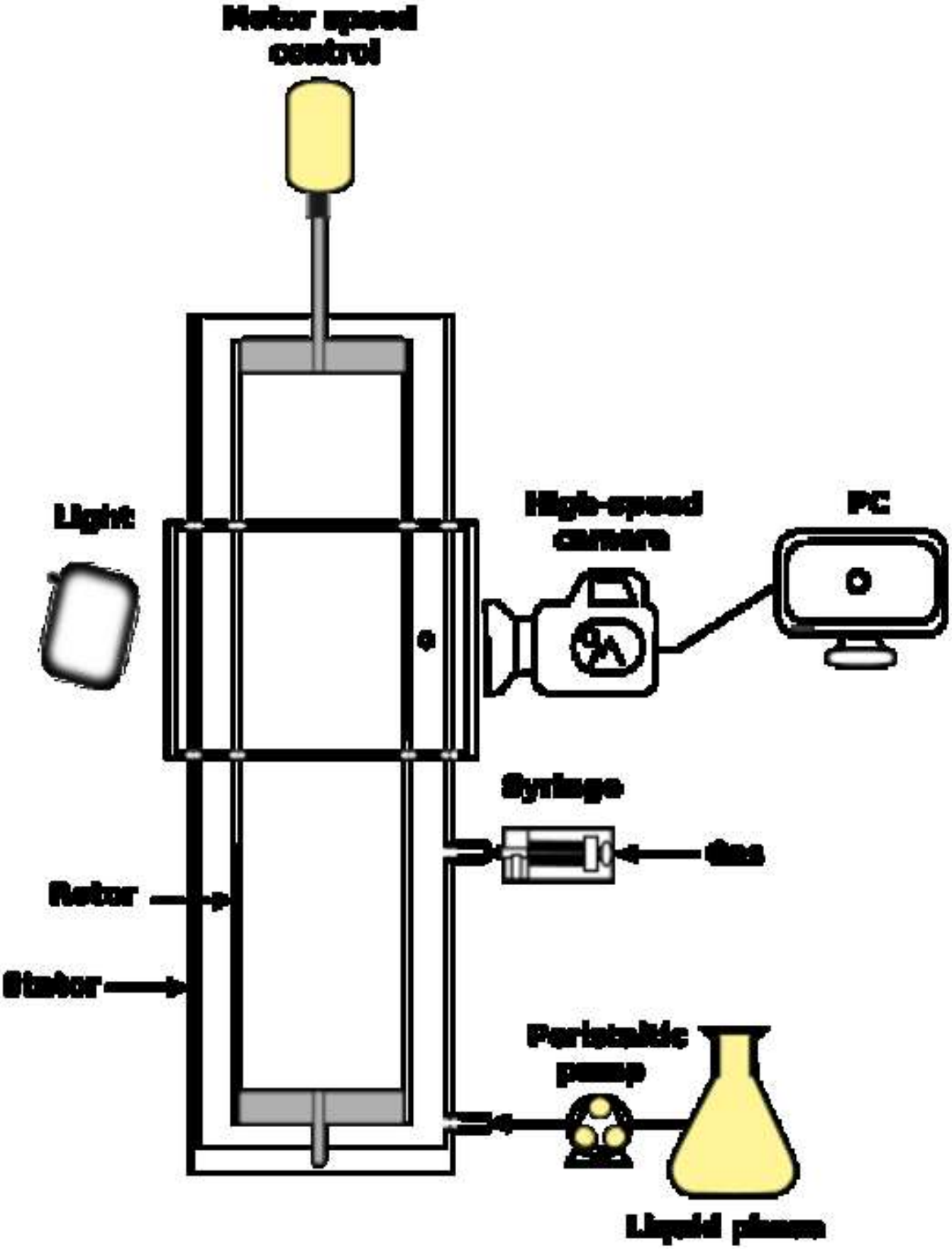

FIGURE 3

Click here to access/download;Figure;FIGURE 3.png

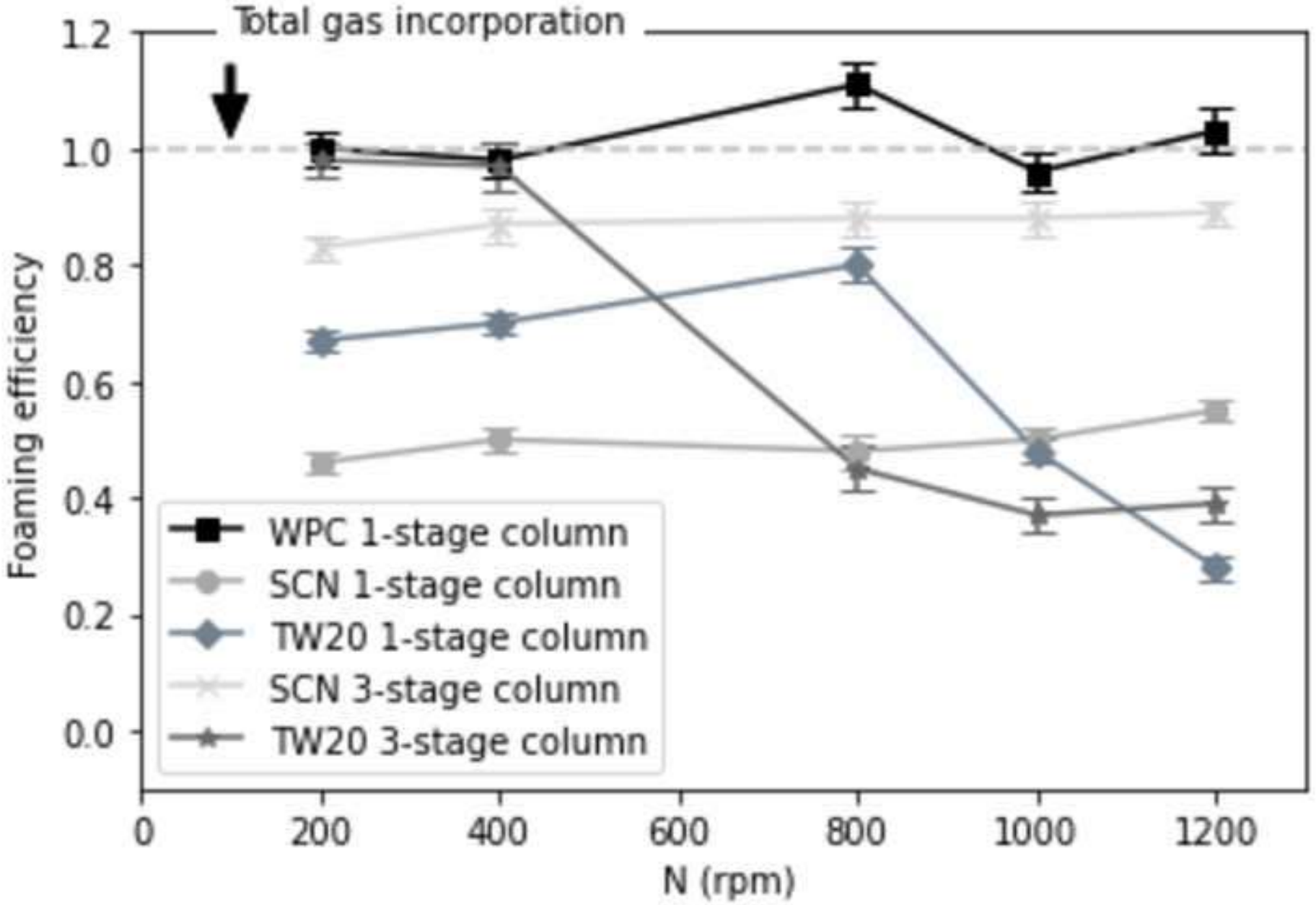

FIGURE 4A

Click here to access/download;Figure;FIGURE 4A.png

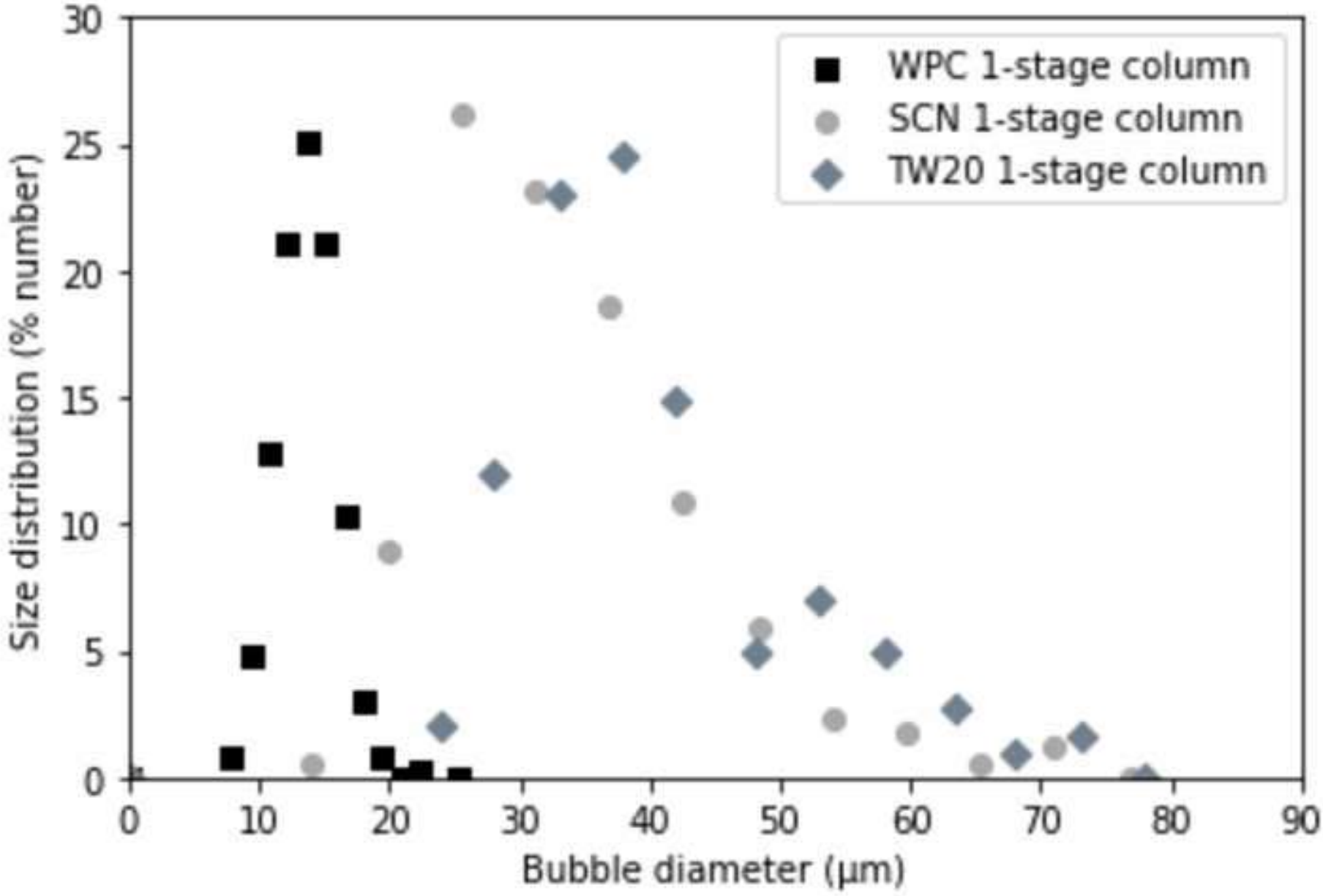

FIGURE 4B

Click here to access/download;Figure;FIGURE 4B.png

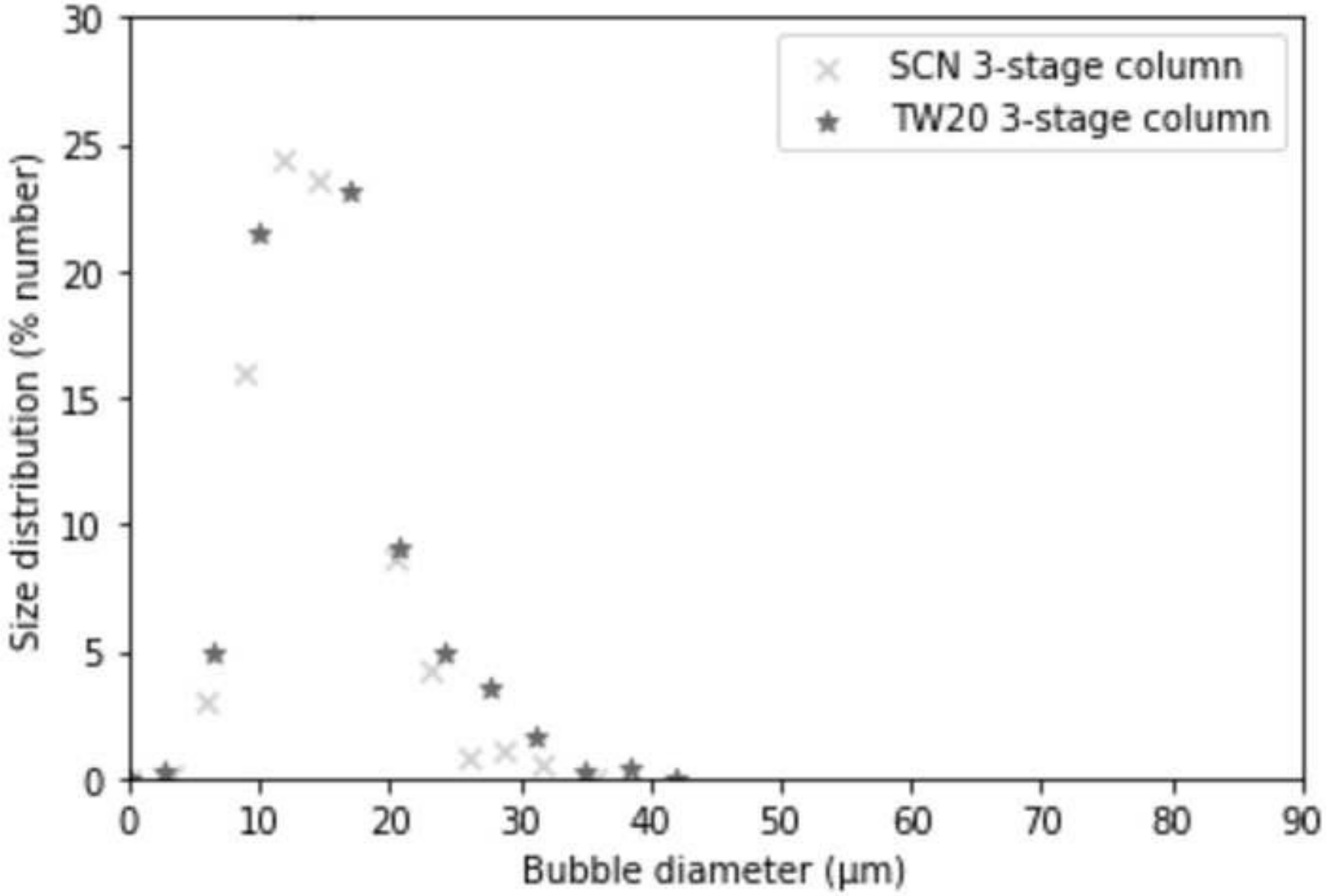

FIGURE 5

Click here to access/download;Figure;FIGURE 5.png

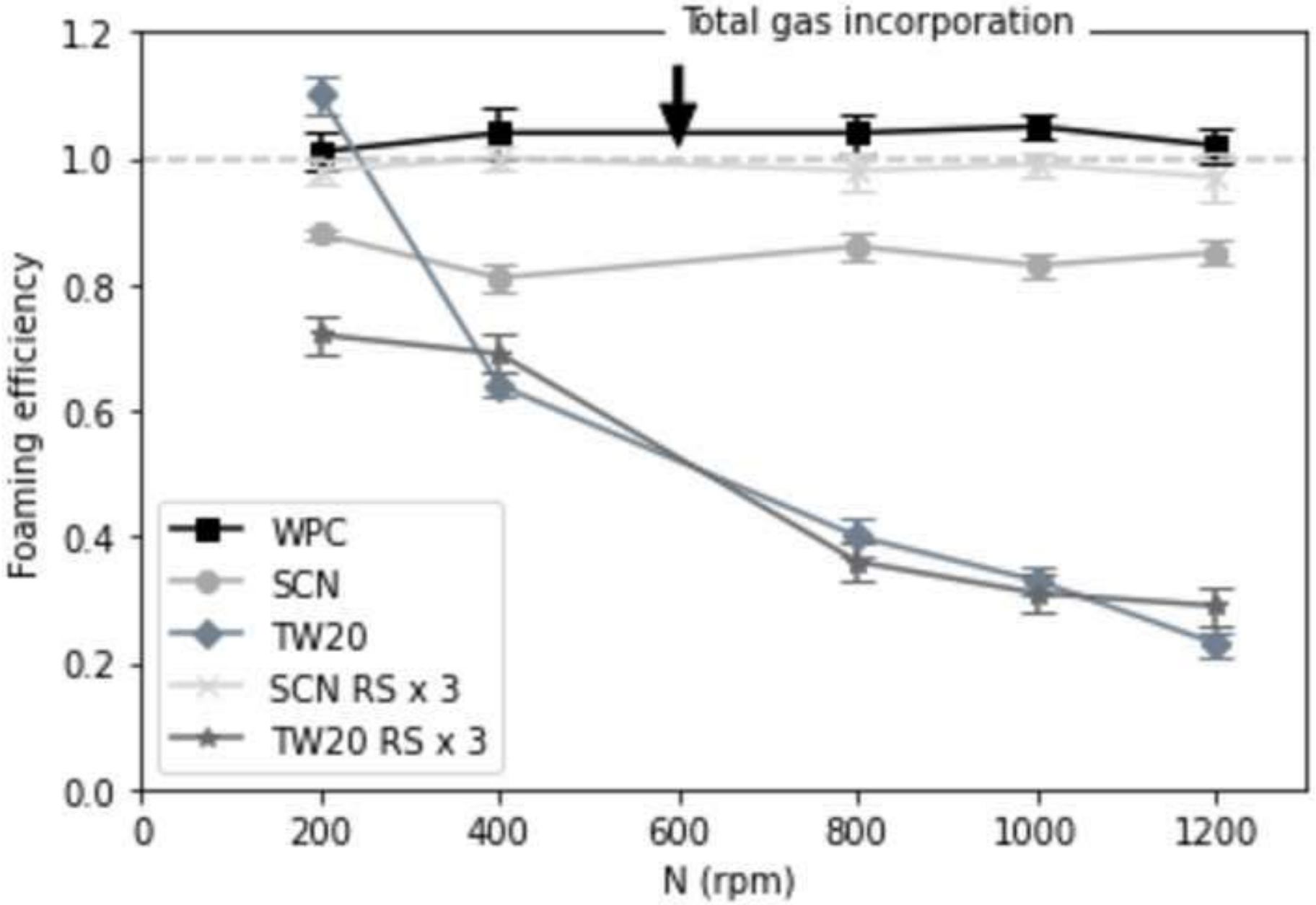

FIGURE 6

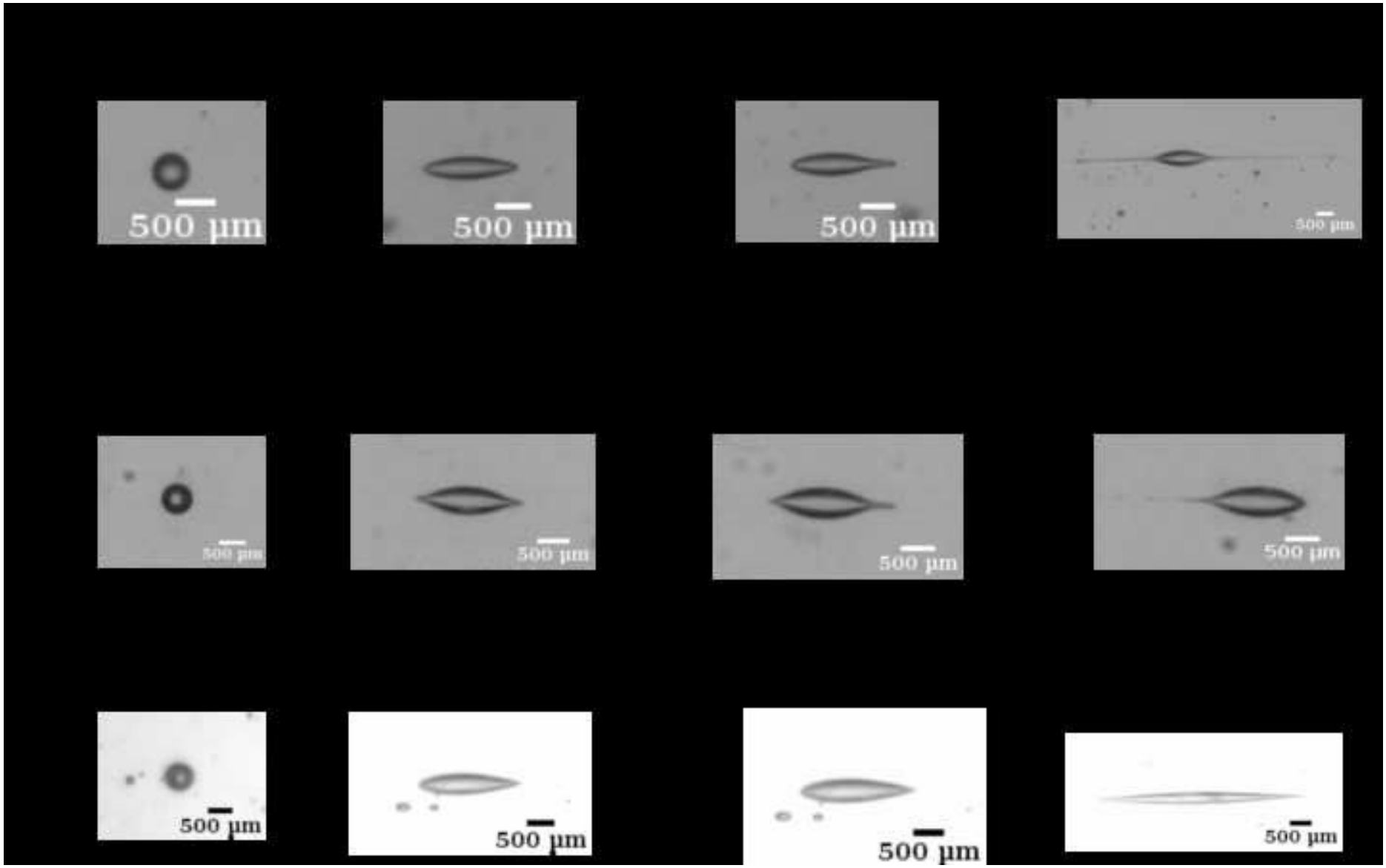

FIGURE 7A

Click here to access/download;Figure;FIGURE 7A.png

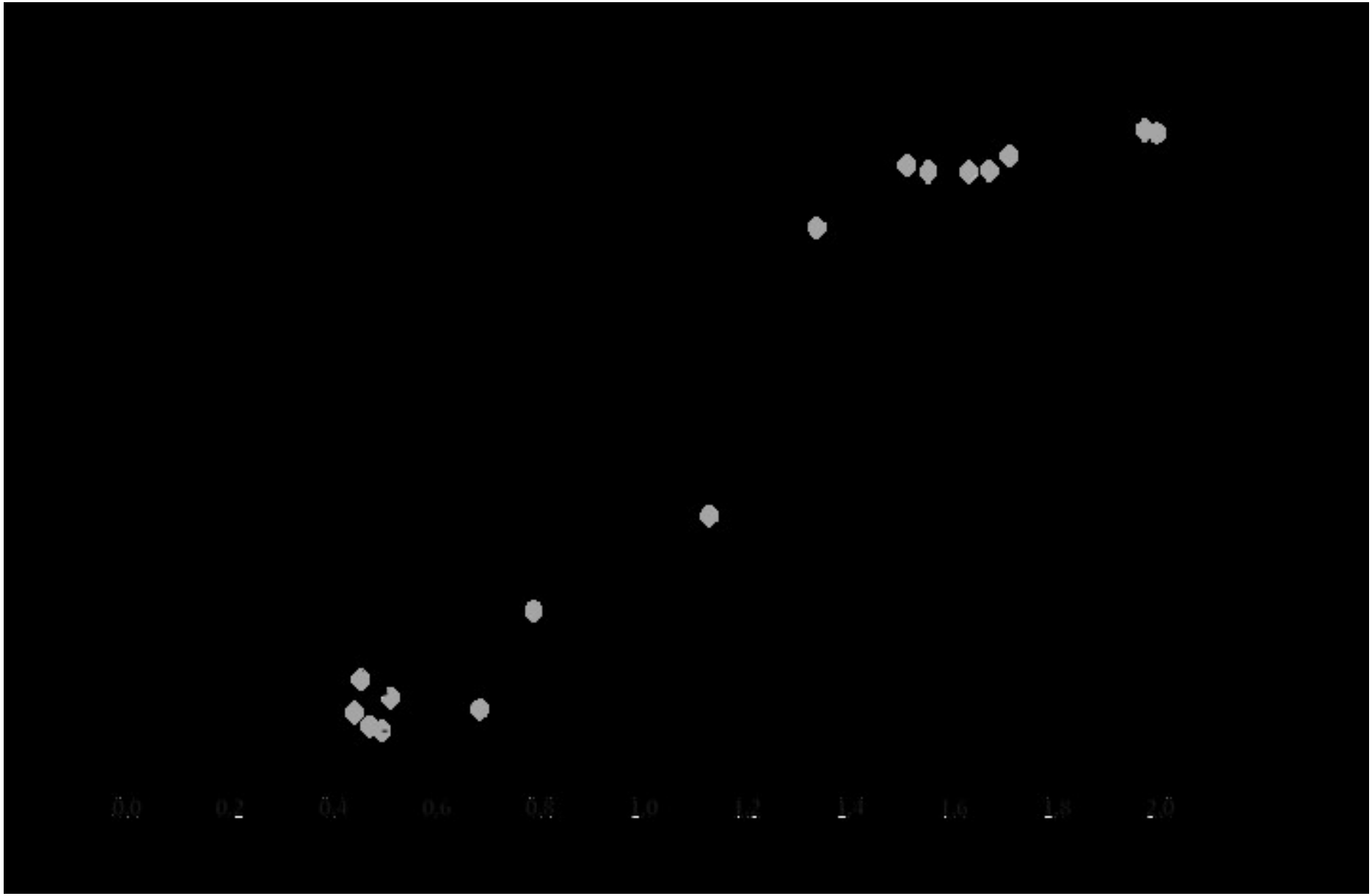

FIGURE 7B

Click here to access/download;Figure;FIGURE 7B.png

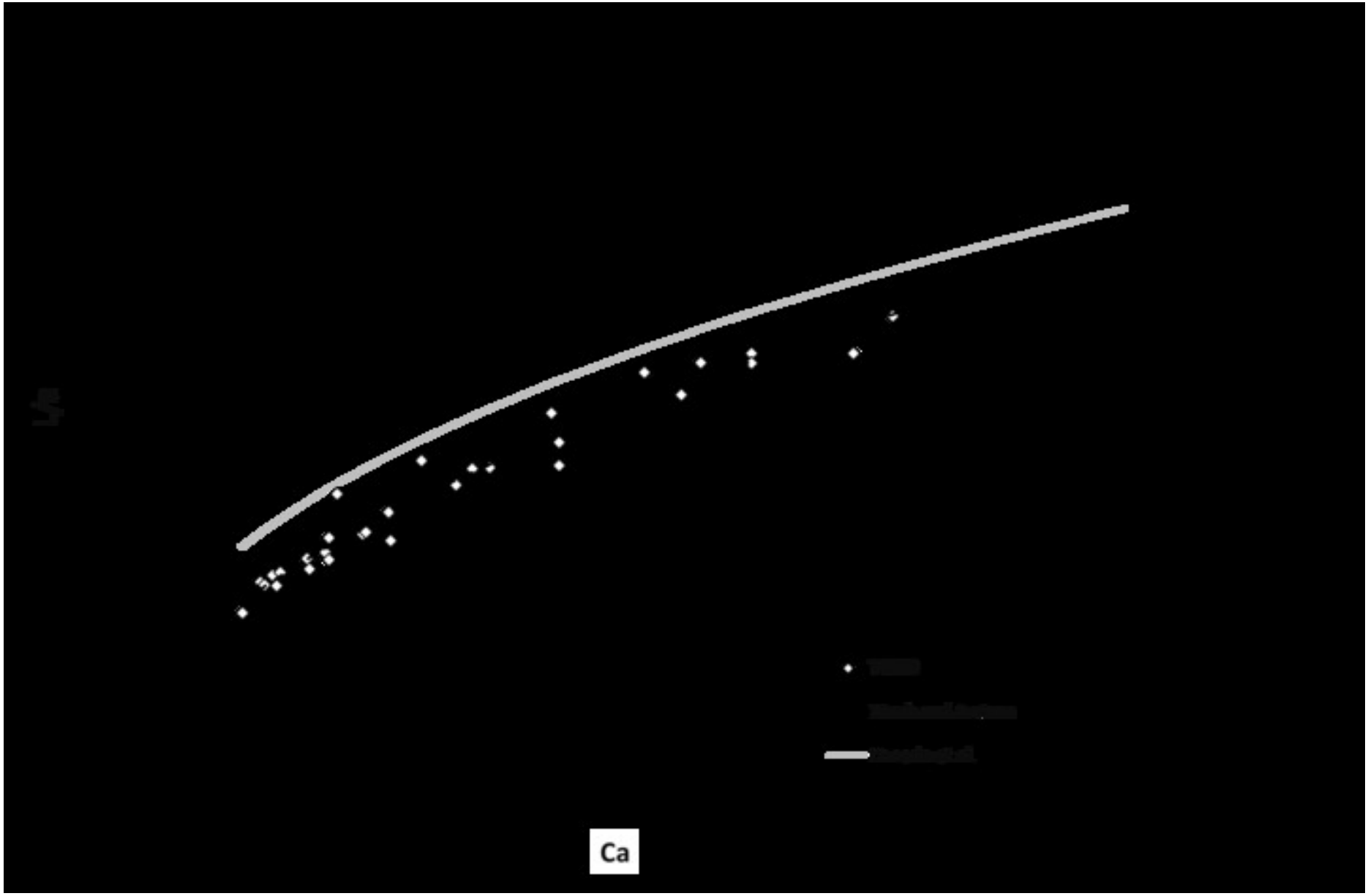

FIGURE 8A

Click here to access/download;Figure;FIGURE 8A.png

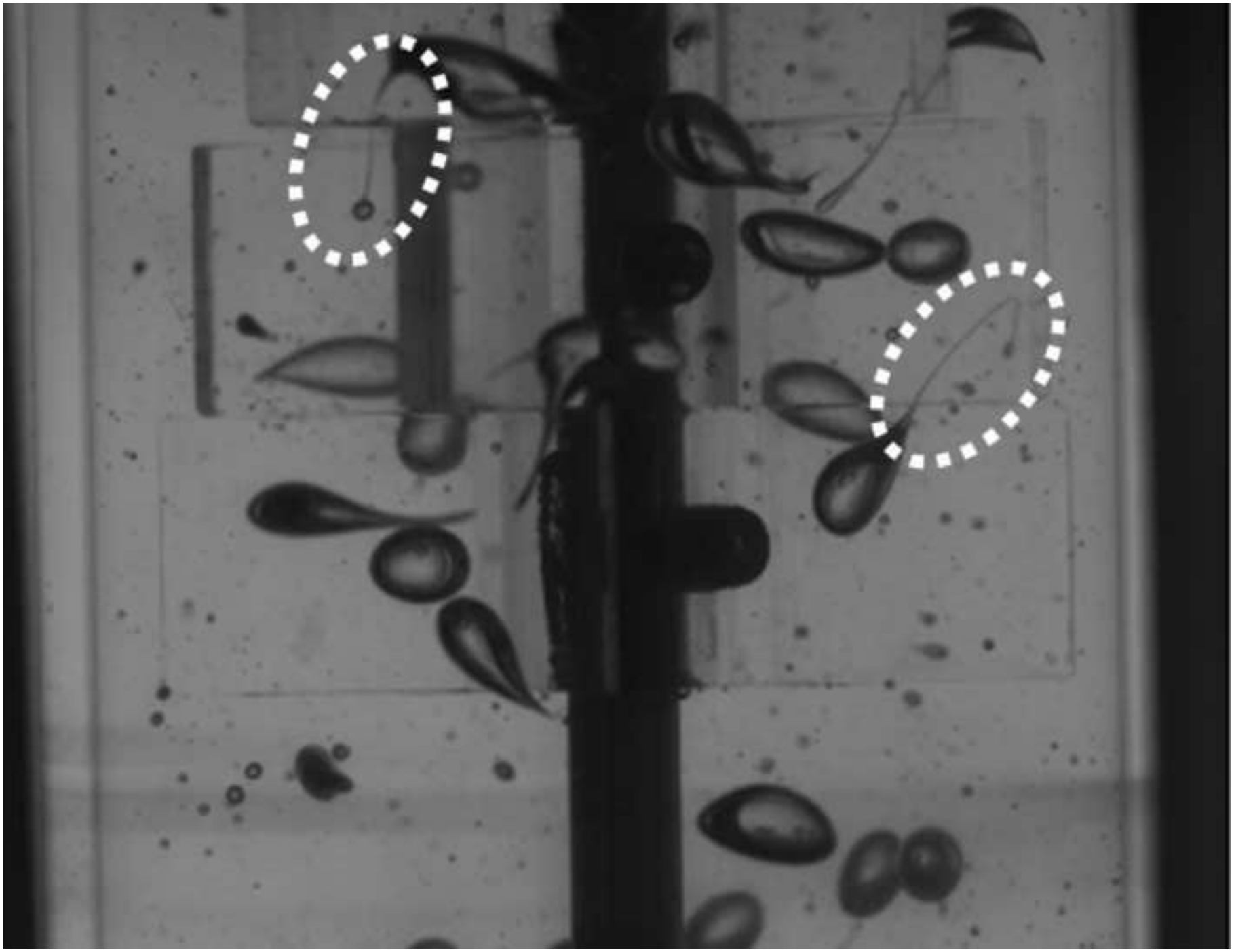

FIGURE 8B

Click here to access/download;Figure;FIGURE 8B.png

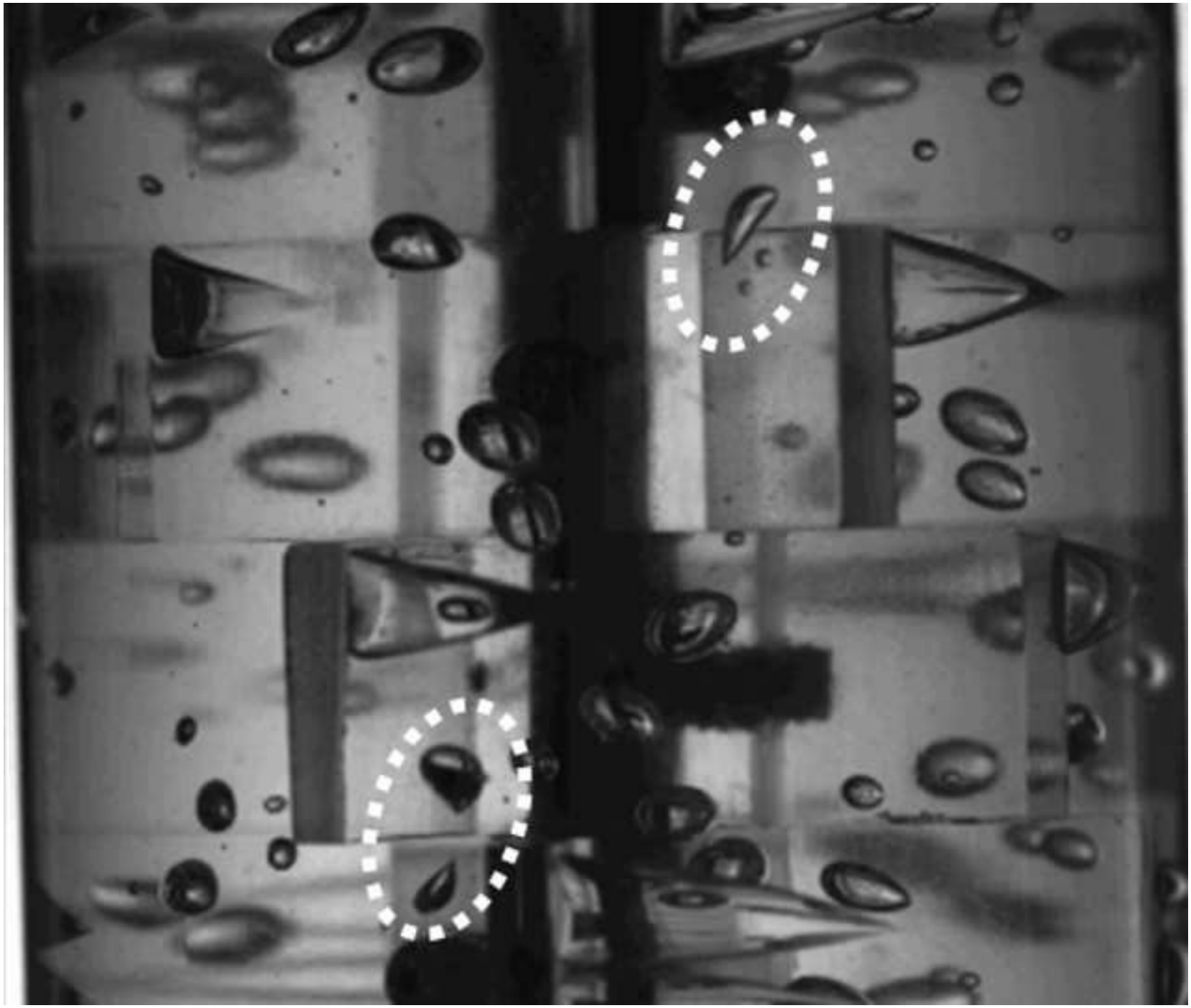

Viscous Newtonian fluid aeration at pilot scale

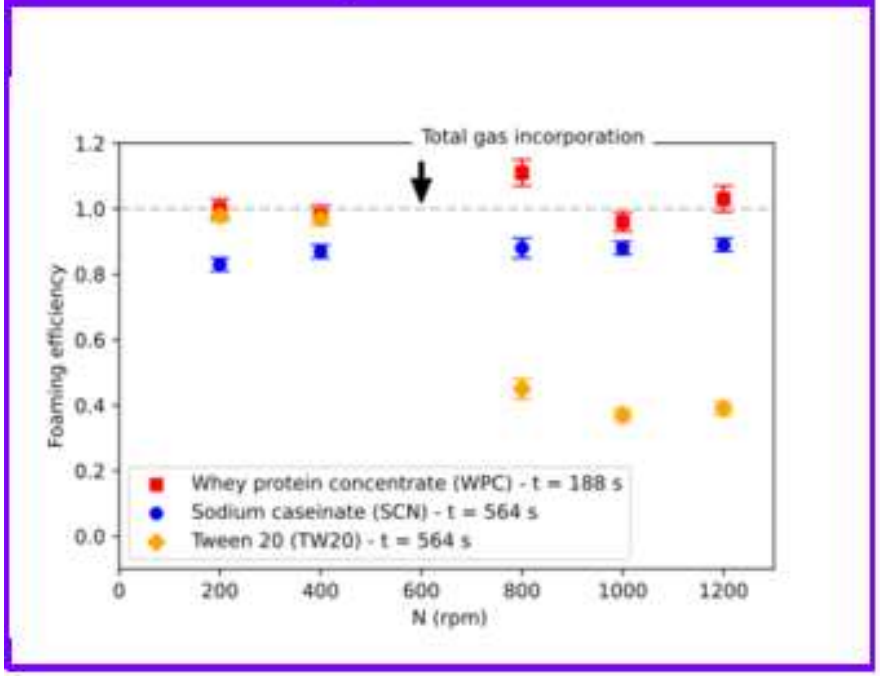

Single bubble deformation and break-up under simple shear

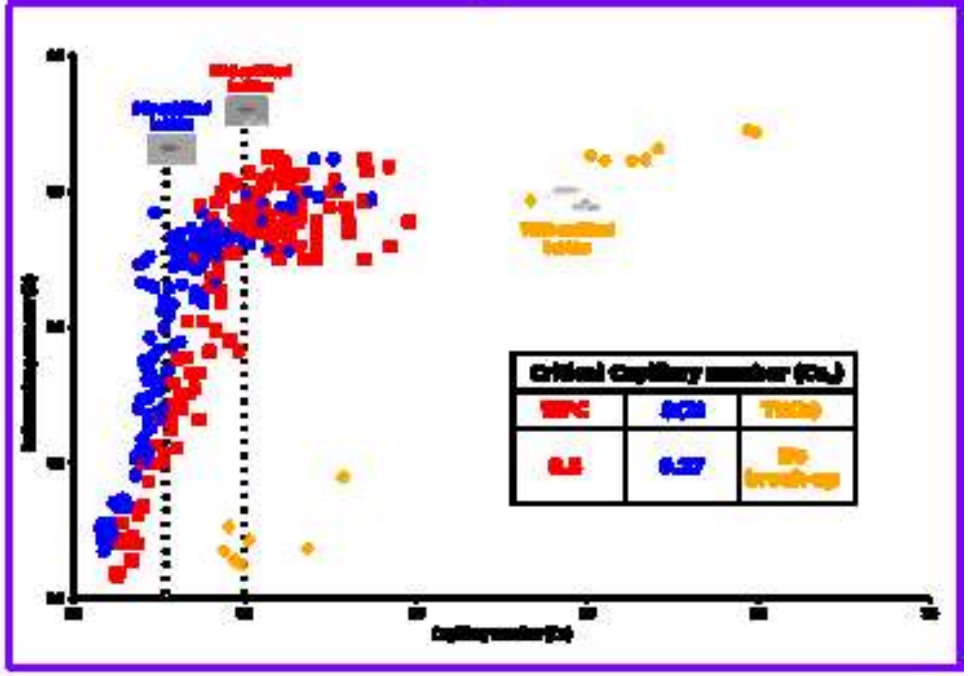

⚓ SCN-stabilized bubbles break at a lower shear rate compared to WPC and yet WPC leads to better pilot-scale foaming efficiency.

⚓ The absence of break-up with TW20 could explain the poor foaming results obtained at pilot scale.

CRediT authorship contribution statement

Boubakar Sanogo: Investigation, Formal Analysis, Software, Data analysis, Writing - original draft. **Kaies Souidi**: Investigation, Formal Analysis, Software, Data analysis. **Alain Marcati**: Conceptualization, Methodology, Validation, Supervision, Writing - review & editing. **Christophe Vial**: Conceptualization, Methodology, Validation, Supervision, Writing - review & editing.

Conflict of Interest form

Declaration of interests

☒The authors declare that they have no known competing financial interests or personal relationships that could have appeared to influence the work reported in this paper.

☐The authors declare the following financial interests/personal relationships which may be considered as potential competing interests: